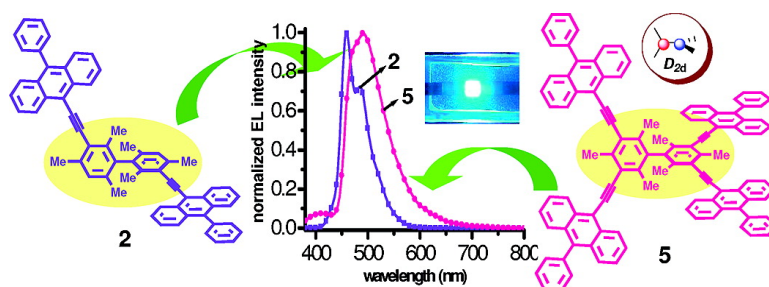


## De Novo Design for Functional Amorphous Materials: Synthesis and Thermal and Light-Emitting Properties of *Twisted* Anthracene-Functionalized Bimesitylenes

Jarugu Narasimha Moorthy, Parthasarathy Venkatakrishnan,  
 Palani Natarajan, Duo-Fong Huang, and Tahsin J. Chow

*J. Am. Chem. Soc.*, **2008**, 130 (51), 17320-17333 • DOI: 10.1021/ja8042905 • Publication Date (Web): 26 November 2008

Downloaded from <http://pubs.acs.org> on February 8, 2009



### More About This Article

Additional resources and features associated with this article are available within the HTML version:

- Supporting Information
- Access to high resolution figures
- Links to articles and content related to this article
- Copyright permission to reproduce figures and/or text from this article

[View the Full Text HTML](#)

## De Novo Design for Functional Amorphous Materials: Synthesis and Thermal and Light-Emitting Properties of Twisted Anthracene-Functionalized Bimesitylenes

Jarugu Narasimha Moorthy,<sup>\*,†</sup> Parthasarathy Venkatakrishnan,<sup>†</sup> Palani Natarajan,<sup>†</sup> Duo-Fong Huang,<sup>‡</sup> and Tahsin J. Chow<sup>\*,‡</sup>

Department of Chemistry, Indian Institute of Technology, Kanpur 208 016, India, and Institute of Chemistry, Academia Sinica, Taipei 115, Taiwan, Republic of China

Received October 4, 2007; E-mail: moorthy@iitk.ac.in (J.N.M.)

**Abstract:** The unique structural attributes inherent to  $D_{2d}$ -symmetric rigid tetraaryl bimesityls render their close packing in the solid state difficult. We have exploited the indisposed tendency of such modules based on the bimesityl scaffold toward crystallization to design a novel class of amorphous functional materials with high glass transition temperatures and thermal stability ( $T_g > 400$  °C). It is shown that a variety of 2- and 4-fold anthracene-functionalized bimesityls, **1–7**, that exhibit excellent amorphous properties ( $T_g =$  ca. 190–330 °C) can be readily prepared via facile Pd(0)-mediated cross-coupling strategies. As the communication between the bimesityl core and the anchored anthracenes is negligible or only marginal, the trends observed for luminescence of model constituent anthracenes are reproduced in the condensed-phase photoluminescence and electroluminescence of **1–7**. In other words, the emission characteristics, i.e.,  $\lambda_{\text{max}}$  and quantum yields, are readily modulated via appropriate modification of the fluorophores. The functional behavior of this unique class of amorphous materials based on the bimesityl scaffold is demonstrated by fabrication of OLED devices. The 2-fold functionalized derivatives **1** and **2** lend themselves to sublimation techniques, so that the electroluminescence is captured with high efficiencies at low turn-on voltages (3.5–6.5 V). The device ITO/NPB (400 Å)/1% **2**:MADN (400 Å)/TPBI (400 Å)/LiF (10 Å)/Al (1500 Å) for **2** yields the highest luminance of  $\sim 13\,900$  cd/m<sup>2</sup> at 17.5 V, a maximum luminance efficiency of  $\sim 7.4$  cd/A at 4.5 V, and a power efficiency of  $\sim 5.3$  lm/W at 4.0 V. Further, at a brightness of 800 cd/m<sup>2</sup> and a current density of 13.8 mA/cm<sup>2</sup>, the device is found to exhibit excellent luminance efficiency of 5.8 cd/A, external quantum efficiency of 4.3% with a power efficiency of 2.2 lm/W, and pure blue light with a CIE<sub>x,y</sub> ( $x = 0.13, y = 0.18$ ). The performance characteristics of the devices fabricated for **1** and **2** are remarkable. Although the 4-fold functionalized systems did not permit sublimation leading to spin-coating as a means for device fabrication, the observed electroluminescence for **4** and **5** attests to a broader scope and applicability of this new category of amorphous molecules for application in OLEDs.

### Introduction

The molecular packing/organization in crystals holds sway on the solid-state properties such as nonlinear optical activity,<sup>1a</sup> ferromagnetic behavior,<sup>1b</sup> conductivity,<sup>1b</sup> thermal and photochemical reactivity,<sup>1c,d</sup> etc.<sup>1</sup> The focus in solid-state organic chemistry over the past 3–4 decades has been to understand the correlation between molecular and crystal structures and progressively achieve *synthesis* of crystals with predetermined molecular ordering based on the attributes of the molecular structures.<sup>2</sup> The “understanding of intermolecular interactions in the context of crystal packing and utilization of such an understanding in the design of new solids with desirable physical

and chemical properties” has been termed *crystal engineering*;<sup>3</sup> indeed, the crystal structures can now be treated as retrosynthetic targets.<sup>4</sup> The flip side of crystal engineering is that the identification of features that thwart crystallization may be elegantly exploited for the development of amorphous molecular materials,<sup>5</sup> which are of immense utility in optoelectronic devices. Extensive investigations on structure–property ( $T_g$ , glass transition temperature) relationships have led to the design of a variety of molecular amorphous materials. Some examples that are of intermediate dimension and exhibit an amorphous property with high  $T_g$  values include tetrahedral, spiro, starburst, dendritic, etc. shaped molecules; cf. Chart 1.<sup>6</sup> Molecules with rigid structural features exhibit packing difficulties, leading to stable amorphous glasses with high morphological stability.<sup>6</sup>

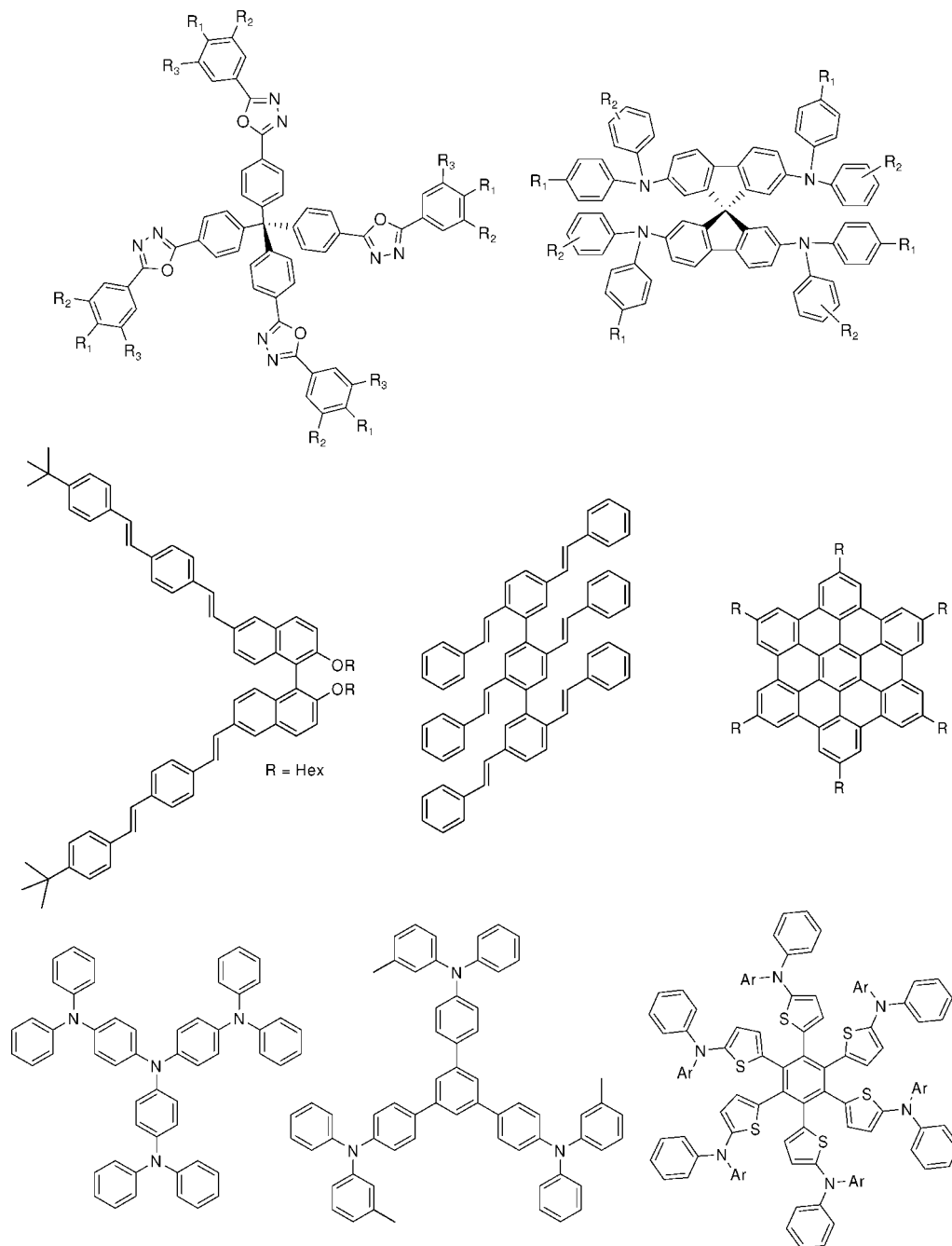
<sup>†</sup> Indian Institute of Technology.

<sup>‡</sup> Academia Sinica.

(1) (a) Evans, O. R.; Lin, W. *Acc. Chem. Res.* **2002**, *35*, 511. (b) Jones, W. *Organic Molecular Solids: Properties and Applications*; CRC Press: Boca Raton, FL, 1998. (c) Toda, F. *Top. Curr. Chem.* **2005**, *254*, 1. (d) Schmidt, G. M. J. *Pure Appl. Chem.* **1971**, *27*, 647–678. (2) Braga, D. *Chem. Commun.* **2003**, 2751.

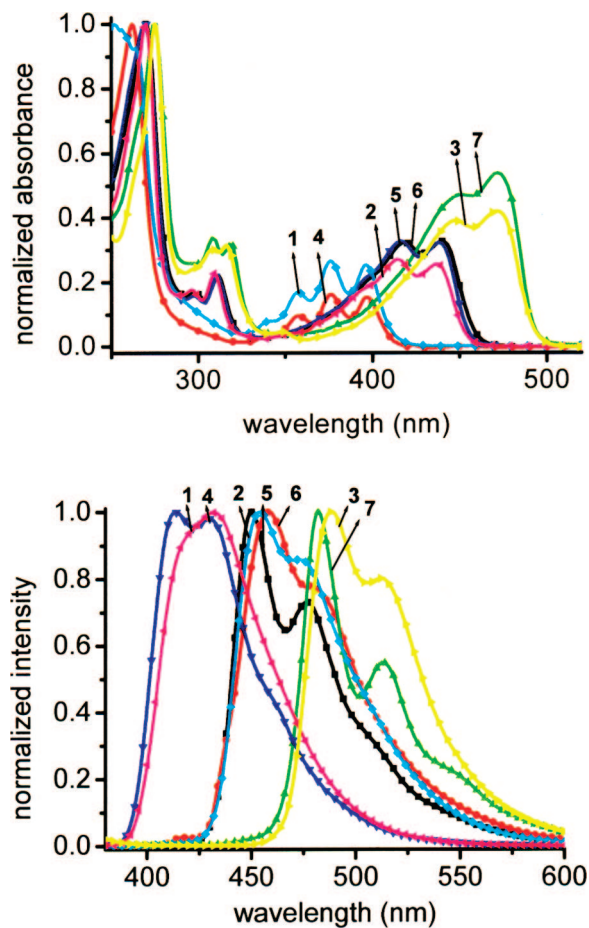
(3) (a) Desiraju, G. R. *Crystal Engineering: The Design of Organic Solids*; Elsevier: Amsterdam, 1989. (b) Lehn, J.-M. *Supramolecular Chemistry: Concepts and Perspectives*; VCH Publishers: New York, 1995. (4) Desiraju, G. R. *Angew. Chem., Int. Ed. Engl.* **1995**, *34*, 2311. (5) Lebel, O.; Maris, T.; Perron, M.-E.; Demers, E.; Wuest, J. D. *J. Am. Chem. Soc.* **2006**, *128*, 10372.

Chart 1. Structures of Typical Amorphous Organic Functional Molecules



We recently reported a de novo design, synthesis, and hydrogen-bonded as well as metal-mediated self-assembly of  $D_{2d}$ -symmetric 3-dimensional modules, viz., tetraarylbimesityls of general structure Tet-Bm shown in Chart 2, into 3-dimensional architectures.<sup>7</sup> The methyl groups at the *ortho* positions of each of the mesitylene rings in bimesitylene render the two rings orthogonal and thus make the core as a whole rigid. The high symmetry and rigidity associated with the arylated modules render the close molecular packing extremely difficult, leading to an amorphous nature. The crystallization was found to occur only when *simple* tetraarylbimesityls contain functional groups such as Br, CN, OH, COOH, etc.; in fact, the hydroxyl- and carboxy-functionalized tetraphenylbimesityls crystallized only in the presence of solvents that may be included in the lattice.<sup>7c</sup> We have failed in our deliberate attempts to crystallize *extended* tetraarylbimesityls. To exploit the indisposed tendency of

3-dimensional extended tetraarylbimesityls to undergo crystallization, we designed anthracene-functionalized bimesityls **1–7** (2-fold as well as 4-fold) as functional amorphous materials for application as emitting materials (EMs) in OLEDs.<sup>8</sup> The latter have been widely studied over the past decade for their application in flat-panel displays and also due to their inherent advantages such as low cost, ease of casting, low turn-on voltages, potential for wide-angle viewing, etc.<sup>9</sup> For application in OLEDs, the materials should ideally permit formation of uniform films (without any pinholes) and exhibit both morphological ( $T_g$ ) and thermal ( $T_d$ ) stability. Thus, in addition to the structural attributes noted above, which impart amorphous nature and high  $T_g$  (due to rigidity and high molecular weight), the following considerations were deemed compelling to explore the potential of anthracene-functionalized bimesitylenes **1–7** as amorphous functional materials.



**Figure 1.** Normalized absorption (left) and emission spectra (right) of the anthracene-anchored bimesitylenes **1–7**.

(1) A serious problem with  $\pi$ -conjugated systems is that the aggregation of planar aromatic systems in thin films depresses the luminescence quantum yield.<sup>10</sup> The most efficient configuration that prevents luminescence quenching in the condensed phase is supposedly the perpendicular orientation of long molecular axes.<sup>11</sup> In all of the anthracene-functionalized bimesitylenes **1–7**, the unique molecular topology was anticipated, a priori, to discourage luminescence quenching. Further, the linkages at the *meta* positions were thought to enhance the charge separation and charge recombination processes in multilayered devices for electroluminescence (EL), as has been reported recently.<sup>12</sup>

(2) Facile functionalization of the bimesityl core (both 2-fold and 4-fold) via Pd(0)-mediated cross-coupling strategies<sup>13</sup> offers the opportunity to access readily a host of compounds.

(3) The potential of anthracenes in EMs has been vastly explored, and the emission maximum of anthracenes can be conveniently tuned by subtle structural modifications.<sup>14</sup> As the communication between the bimesityl core and the anchored anthracenes is negligible or virtually nonexistent, the trends observed for luminescence of various derivatives were expected to be reproduced in the condensed-phase photoluminescence and electroluminescence.

## Results

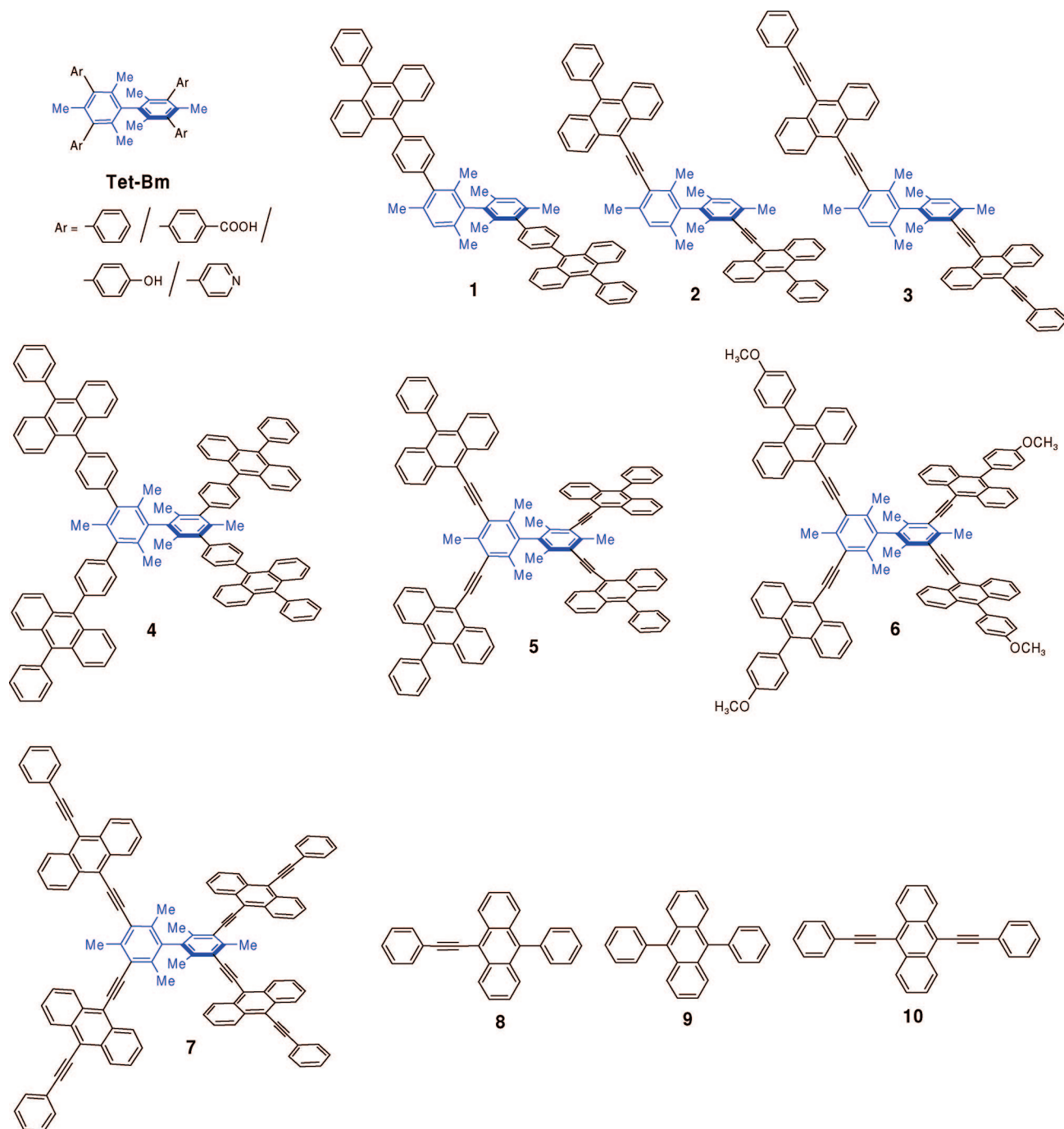
**Synthesis of the 2- and 4-Fold Anthracene-Anchored Bimesityls 1–7.** The preparation of **1–7** (Chart 1) was accomplished according to the synthetic routes given in Scheme

1. Diiodination of bimesityl<sup>7c</sup> with *N*-iodosuccinimide in the presence of a catalytic amount of trifluoroacetic acid afforded 3,3'-diiodobimesityl in 83% yield (Scheme 1). 2-fold functionalization of the bimesitylene was achieved via Pd(0)-mediated Sonogashira coupling between 3,3'-diiodobimesityl and (trimethylsilyl)acetylene. The subsequent deprotection using tetrabutylammonium fluoride (TBAF) afforded 3,3'-diethynylbimesityl in near quantitative yield. The Suzuki and Sonogashira coupling of 3,3'-diiodobimesityl and 3,3'-diethynylbimesityl with the corresponding coupling partners yielded **1–3** in 41–62% yields (Scheme 1).

Tetraiodination of the readily prepared bimesityl with I<sub>2</sub> in an AcOH/HNO<sub>3</sub>–H<sub>2</sub>SO<sub>4</sub> mixture yielded tetraiodobimesityl (**11**).<sup>7c</sup> 4-Fold functionalization of the bimesityl core by four anthracene moieties was successfully achieved via Pd(0)-mediated Suzuki/Sonogashira coupling reactions. Thus, the anthracene derivative **5** was synthesized starting from the 3,3',5,5'-tetraethynylbimesityl (**12**), which in turn was readily prepared from Sonogashira coupling of tetraiodobimesityl and (trimethylsilyl)acetylene followed by deprotection of the TMS group with TBAF (Scheme 1). The 4-fold Sonogashira coupling between tetraethynylbimesityl and 9-bromo-10-phenylanthracene (**15**) using Pd(0) as a catalyst, CuI as a cocatalyst, and Et<sub>3</sub>N as a solvent led to isolation of **5** in 59% yield. In a similar manner, the coupling reaction of 9-bromo-10-(4-methoxyphenyl)anthracene (**16**) and 9-bromo-10-(phenylethynyl)anthracene (**17**) with tetraethynylbimesityl afforded the elaborated anthracene derivatives **6** and **7** in 52% and 54% yields, respectively (Scheme 1). The 4-fold diphenylanthracene-derivatized bimesityl **4** was obtained in good yields from the Suzuki coupling reaction between **15** and the tetraboronate ester **13**. Whereas the model compounds **9** and **10** were commercially available, compound **8** was synthesized using 9-bromo-10-phenylanthracene and phenylacetylene via Sonogashira coupling. All the compounds

- (6) For 1,3,5-triarylbenzene- and triarylamine-based systems, see: (a) Shirota, Y. *J. Mater. Chem.* **2000**, *10*, 1. (b) Thelakkat, M. *Macromol. Mater. Eng.* **2002**, *287*, 442. (c) Shirota, Y. *J. Mater. Chem.* **2005**, *15*, 75. (d) Forrest, S. R.; Thompson, M. E. *Chem. Rev.* **2007**, *107*, 923–1386. For spirobifluorene-based systems, see: (e) Salbeck, J.; Yu, N.; Bauer, J.; Weissörtel, F.; Bestgen, H. *Synth. Met.* **1997**, *91*, 209. (f) Johansson, N.; Salbeck, J.; Bauer, J.; Weissörtel, F.; Broms, P.; erson, A.; Salaneck, W. R. *Adv. Mater.* **1998**, *10*, 1136. (g) Kim, Y.-H.; Shin, D.-C.; Kim, S.-H.; Ko, C.-H.; Yu, H.-S.; Chae, Y.-S.; Kwon, S.-K. *Adv. Mater.* **2001**, *13*, 1690. (h) Shen, W.-J.; Dodda, R.; Wu, C.-C.; Wu, F.-I.; Liu, T.-H.; Chen, H.-H.; Chen, C. H.; Shu, C.-F. *Chem. Mater.* **2004**, *16*, 930. For tetraarylmethane-based systems, see: (i) Robinson, M. R.; Wang, S.; Bazan, G. C.; Cao, Y. *Adv. Mater.* **2000**, *12*, 1701. (j) Wang, S.; Oldham, W. J., Jr.; Hudack, R. A., Jr.; Bazan, G. C. *J. Am. Chem. Soc.* **2000**, *122*, 5695. (k) Robinson, M. R.; Wang, S.; Heeger, A. J.; Bazan, G. C. *Adv. Funct. Mater.* **2001**, *11*, 413. For hexaarylbenzene-based systems, see: (l) Wu, I.-Y.; Lin, J. T.; Tao, Y.-T.; Balasubramaniam, E. *Adv. Mater.* **2000**, *12*, 668. (m) Thomas, K. R. J.; Velusamy, M.; Lin, J. T.; Chuen, C. H.; Tao, Y.-T. *J. Mater. Chem.* **2005**, *15*, 4453. For benzocoronene-based hole-transporting systems, see: (n) Wu, J.; Baumgarten, M.; Debije, M. G.; Warman, J. M.; Mullen, K. *Angew. Chem., Int. Ed.* **2004**, *43*, 5331. For binaphthyl-based systems, see: (o) Ostrowski, J. C.; Hudack, R. A., Jr.; Robinson, M. R.; Wang, S.; Bazan, G. C. *Chem.—Eur. J.* **2001**, *7*, 4500. (p) Benmansour, H.; Shioya, T.; Sato, Y.; Bazan, G. C. *Adv. Funct. Mater.* **2003**, *13*, 883. (q) He, Q.; Lin, H.; Weng, Y.; Zhang, B.; Wang, Z.; Lei, G.; Wang, L.; Qiu, Y.; Bai, F. *Adv. Funct. Mater.* **2006**, *16*, 1343. For biphenyl-based systems, see: (r) He, F.; Cheng, G.; Zhang, H.; Zheng, Y.; Xie, Z.; Yang, B.; Ma, Y.; Liu, S.; Shen, J. *Chem. Commun.* **2003**, 2206. (s) He, F.; Xia, H.; Tang, S.; Duan, Y.; Zheng, M.; Liu, L.; Li, M.; Zhang, H.; Yang, B.; Ma, Y.; Liu, S.; Shen, J. *J. Mater. Chem.* **2004**, *14*, 2735. (t) He, F.; Xu, H.; Yang, B.; Duan, Y.; Tian, L.; Huang, K.; Ma, Y.; Liu, S.; Feng, S.; Shen, J. *Adv. Mater.* **2005**, *17*, 2710. (u) Xie, Z.; Yang, B.; Li, F.; Cheng, G.; Liu, L.; Yang, G.; Xu, H.; Ye, L.; Hanif, M.; Liu, S.; Ma, D.; Ma, Y. *J. Am. Chem. Soc.* **2005**, *127*, 14152.

Chart 2. Structures of Amorphous Functional Materials 1–7 Based on a Bimesityl Core



were purified by silica gel column chromatographic techniques. The starting materials, i.e., **15** and **16**, were prepared by following the reported procedures.<sup>15a,b</sup> The compound **17** was prepared by Sonogashira coupling of 9,10-dibromoanthracene with phenylacetylene.<sup>15c</sup> The boronic acid of diphenylanthracene (**14**) was prepared from 9-(4-bromophenyl)-10-phenylanthracene, which in turn was prepared from 9-phenylanthracene boronate ester; cf. the Supporting Information (SI).

All the intermediate compounds were characterized routinely by <sup>1</sup>H and <sup>13</sup>C NMR spectroscopies, and the 2-fold/4-fold functionalized anthracene derivatives **1–7** were characterized by IR, <sup>1</sup>H and <sup>13</sup>C NMR, MS, and CHN analyses.

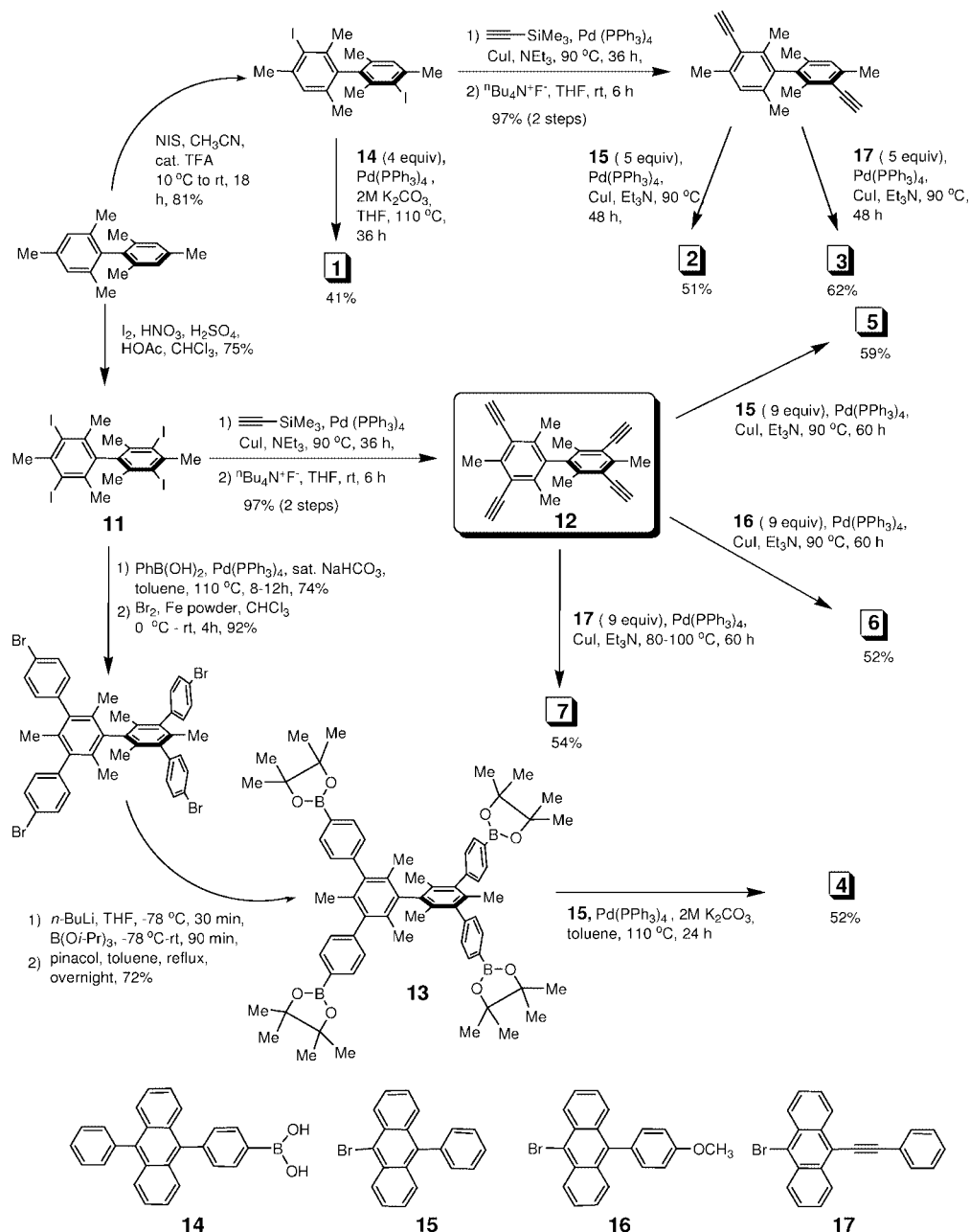
**Photophysical Studies.** The normalized UV–vis absorption spectra for **1–7** are shown in Figure 1, a perusal of which shows

(7) (a) Natarajan, R.; Savitha, G.; Moorthy, J. N. *Cryst. Growth Des.* **2005**, *5*, 69. (b) Natarajan, R.; Savitha, G.; Dominiak, P.; Wozniak, K.; Moorthy, J. N. *Angew. Chem., Int. Ed.* **2005**, *44*, 2115. (c) Moorthy, J. N.; Natarajan, R.; Venugopalan, P. *J. Org. Chem.* **2005**, *70*, 8568. (d) Moorthy, J. N.; Natarajan, R.; Savitha, G.; Venugopalan, P. *Cryst. Growth Des.* **2006**, *6*, 919.

(8) In our recent preliminary investigations, we have shown that diarylaminobiphenyl-functionalized bimesityls serve as blue light emitting materials; see: (a) Moorthy, J. N.; Venkatakrishnan, P.; Huang, D.-F.; Chow, T. J. *Chem. Commun.* **2008**, 2146.

(9) (a) *Organic Electroluminescence*; Kafafi, Z. H., Ed.; Optical Engineering Vol. 94; Taylor and Francis: Boca Raton, FL, 2005. (b) Shirota, Y. In *Organic Electroluminescence*; Kafafi, Z. H., Ed.; Optical Engineering, Vol. 94; Taylor and Francis: Boca Raton, FL, 2005; Chapter 4, p 147.

## Scheme 1. Synthesis of Anthracene-Functionalized Bimesitylenes 1–7



that the absorptions differ significantly depending on the substitution of the anthracene moieties. The anthracene-anchored bimesityls **1–7** exhibit a common short-wavelength absorption band at ca. 280 nm and a long-wavelength band, whose absorption maximum varies depending on the nature of the anthracene moiety. The absorption features are similar for pairs **1** and **4** and **3** and **7**. Likewise, **2**, **5**, and **6** exhibit similar features. The molar extinction coefficients ( $\epsilon$ ) of the 4-fold derivatives at the absorption maxima were found to be almost twice that for 2-fold functionalized derivatives. For example, the  $\epsilon$  values for **1** and **4** are 57 200 (390 nm) and 123 820 (390 nm)  $\text{M}^{-1} \text{cm}^{-1}$ , respectively. A similar trend was observed for the pairs **2** and **5** and **3** and **7**. The optical band gap values ( $E_g^{\text{opt}}$ , eV) for **1–7** were determined from their absorption onset potential edge of the absorption spectra (Table 1). These values vary from 2.47 to 2.98 eV; cf. Table 1.

The excitation spectra recorded for **1–7** at two different wavelengths were found to be similar to those of the absorption spectra. To examine the fluorescence properties of anthracene-anchored bimesityls **1–7**, the photoluminescence (PL) studies

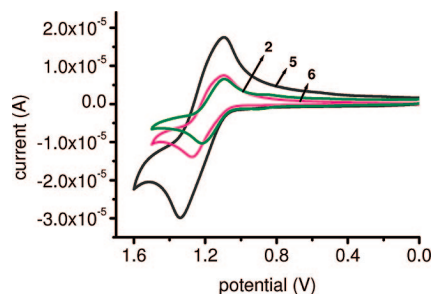


**Figure 2.** Typical cyclic voltammograms (oxidation waves) observed for the anthracene derivatives **2**, **5**, and **6** in dichloromethane/0.1 M TBAP.

**Table 1.** Optical Absorption, PL, PL Quantum Yields, and Thermal Properties of Compounds 1–10

compd	$\lambda_{\max}^{\text{abs}}$ (nm) ( $\epsilon \times 10^5$ ) <sup>a</sup>	band gap, <sup>b</sup> $\lambda$ (eV)	$\lambda_{\max}^{\text{f}}(\text{solution})^c$ (nm)	$\lambda_{\max}^{\text{f}}(\text{film})^d$ (nm)	$\Phi_{\text{fl}}(\text{solution})^e$	$T_d^f$ (°C)	$T_g^g$ (°C)
1	396 (0.57)	420, 2.95	432 (460 s)	455	0.84	518	191
2	436 (1.63)	458, 2.71	453 (476, 504 s)	502	0.59	430	297
3	471 (0.54)	501, 2.47	488 (512, 552 s)	572	0.55	422	247
4	397 (1.23)	416, 2.98	430 (463 s)	447	0.76	471	234
5	438 (2.36)	460, 2.69	450 (477, 508 s)	493	0.86	485	244
6	440 (2.19)	464, 2.67	456 (481, 510 s)	486	0.75	455	202
7	472 (1.10)	504, 2.46	485 (514, 550 s)	547	0.57	486	330
8	425	446, 2.78	441	499	0.92	283	153, 207 <sup>h</sup>
9	375 <sup>i</sup>		430 <sup>i</sup>		0.96 <sup>i</sup>	260	190, 248 <sup>h</sup>
10	440 <sup>j</sup>		507 <sup>j</sup>		0.88 <sup>j</sup>	466	–, <sup>k</sup> 250 <sup>h</sup>

<sup>a</sup> The molar extinction coefficients were determined for dichloromethane solutions (ca.  $1 \times 10^{-5}$  M) at 390 nm. <sup>b</sup> Band gap values as calculated from the onset potential ( $\lambda$ ) of the absorption spectrum; see the text. <sup>c</sup> All the emission spectra were recorded for dilute solutions ( $1 \times 10^{-6}$  M) in cyclohexane; the values in parentheses refer to other absorption bands and shoulders (s). <sup>d</sup> All the films were prepared by spin-coating of the solutions in 1,2-dichloroethane. <sup>e</sup> Quantum yields were calculated using anthracene as a standard and N<sub>2</sub>-bubbled cyclohexane as a solvent for  $\lambda_{\text{ex}} = 367$  nm. The reported values are an average of three independent determinations. <sup>f</sup> Obtained from thermogravimetric analysis under argon/nitrogen gas at a heating rate of 10 or 5 °C/min. <sup>g</sup> Obtained from differential scanning calorimetry under argon/nitrogen gas at a heating rate of 10 or 5 °C/min. <sup>h</sup> Melting points from the literature are given for comparison. <sup>i</sup> Reference 16. <sup>j</sup> Reference 17. <sup>k</sup> Not available.

were carried out on dilute solutions ( $1 \times 10^{-6}$  M, Figure 1) and thin films (solid state); cf. the SI. The results are collected in Table 1. The emission maximum for **1** and **4** in the solution state was observed at ca. 430 nm, which is blue. For **2** and **5** blue-green emissions were observed with maxima at 453 and 450 nm. The anthracene derivatives **3** and **7** were found to emit in the green region with  $\lambda_{\max}$  at ca. 485–488 nm. The model compound **8** showed an emission maximum at 441 nm. From the spectra in Figure 1, one clearly observes a red shift in the emission maximum for **7** relative to that for **5** and **6** by ca. 30–35 nm.

The PL studies on films were also performed to examine the emission in the condensed phase. The films were made by spin-casting of their solutions in 1,2-dichloroethane onto the quartz plates. The films of bimesitylenes **1**, **2**, and **4** exhibited red-shifted emission by ca. 20–50 nm as compared to the emission in the solution state. The emission maxima for the films of **5** and **6** were found to be ca. 40 nm red-shifted from those observed in their solution states. A red shift by ca. 60–80 nm with a slight broadening toward the longer wavelength region was observed for **3** and **7** (cf. the SI). The red shifts in the emission maxima of **1**, **2**, and **4–6** by ca. 20–50 nm in the spin-coated films is presumably due to varying degrees of planarization of the phenyl/aryl rings with respect to central anthracene rings within the amorphous phase; this may result in a continuum of states that disturb the vibronic pattern, leading to a broad red-shifted emission. The sterically hindered phenyl/aryl rings cannot be expected to promote excimer formation.<sup>18</sup> The fact that one observes a structured photoluminescence as well as electroluminescence for vacuum-deposited films, e.g.,

for **2** (cf. the SI), lends credence to this.<sup>19</sup> Furthermore, the excitation spectra typically recorded for the film of **2** at various wavelengths of emission maximum were identical. For bimesitylenes **3** and **7**, it is likely that the extended phenylethynyl arms of the neighboring molecules within the amorphous phase penetrate into each other, leading to partial charge transfer in the excited state, which manifests in observed red-shifted emission with associated broadening. It should be noted that, even for these cases, excimer formation via cofacial arrangement of the (phenylethynyl)anthracene chromophores cannot occur due to the bimesityl scaffold. For all bimesitylenes **1–7**, the difference in the dielectric constants of the two media, i.e., solution and thin film, may additionally contribute to the observed red-shifted emissions upon going from solutions to films.<sup>20</sup> The photoluminescence quantum yields ( $\Phi_{\text{fl}}$ ) for **1–7** were determined in cyclohexane using anthracene as a standard,<sup>21</sup> and the results are recorded in Table 1. The efficiencies for **1–7** fall in the range 0.55–0.86 and are comparable to those of their respective model compounds **8–10**.<sup>22</sup>

**Thermal Properties.** The thermal behavior of the anthracene-anchored bimesityls **1–7** was examined by TGA and DSC studies. All the compounds were found to exhibit a high decomposition temperatures ( $T_d$ ) in the range between 420 and 520 °C; cf. the SI. In contrast, the simple model compounds **8–10** are characterized by relatively low melting points. One observes a regular improvement in the thermal stability as we move from disubstituted bimesitylene **2** to simple phenylanthracene-substituted bimesitylene **5** to the bulky (phenylethynyl)anthracene-substituted bimesityl derivative **7** (Table 1). The

- (10) (a) Kasha, M.; Rawls, H. R.; Bayoumi, M. A. *Pure Appl. Chem.* **1965**, *11*, 371. (b) Jenekhe, S. A.; Osaheni, J. A. *Science* **1994**, *27*, 7. (c) Moffitt, M.; Farinha, J. P. S.; Winnik, M. A.; Rohr, U.; Müllen, K. *Macromolecules* **1999**, *32*, 4895. (d) Würthner, F.; Thalacker, C.; Dieke, S.; Tschierske, C. *Chem.—Eur. J.* **2001**, *7*, 2245.
- (11) (a) Cornil, J.; Beljonne, D.; Calbert, J. P.; Brédas, J. L. *Adv. Mater.* **2001**, *13*, 1053. (b) Hallenx, V. de.; Calbert, J. P.; Brocorens, P.; Cornil, J.; Delercq, J. P.; Brédas, J. L. *Adv. Funct. Mater.* **2004**, *14*, 649. (c) Cornil, J.; dos Santos, D. A.; Crispin, X.; Silbey, R.; Brédas, J. L. *J. Am. Chem. Soc.* **1998**, *120*, 1289. (d) Xie, Z.; Yang, B.; Li, F.; Cheng, G.; Liu, L.; Yang, G.; Xu, H.; Ye, L.; Hanif, M.; Liu, S.; Ma, D.; Ma, Y. *J. Am. Chem. Soc.* **2005**, *127*, 14152.
- (12) Thompson, A. L.; Ahn, T. S.; Thomas, K. R. J.; Thayumanavan, S.; Martinez, T. J.; Bardeen, C. J. *J. Am. Chem. Soc.* **2005**, *127*, 16348.
- (13) (a) Negishi, E.-i., Ed. *Handbook of Organopalladium Chemistry for Organic Synthesis*; Wiley Interscience: New York, 2002. (b) Miyaura, N., Ed. *Cross-Coupling Reactions: A Practical Guide*; Topics in Current Chemistry Series 219; Springer Verlag: New York, 2002.

- (14) For example, see: (a) Kim, Y. H.; Shin, D. C.; Kim, S. H.; Ko, C. H.; Yu, H. S.; Chae, Y. S.; Kwon, S. K. *Adv. Mater.* **2001**, *13*, 1690. (b) Kim, Y. H.; Jeong, H. C.; Kim, S. H.; Yang, K.; Kwon, S. K. *Adv. Funct. Mater.* **2005**, *15*, 1799. (c) Zheng, S.; Shi, J. *Chem. Mater.* **2001**, *13*, 4405. (d) Klärner, G.; Davey, M. H.; Chen, W. D.; Scott, J. C.; Miller, R. D. *Adv. Mater.* **1998**, *10*, 993.
- (15) (a) Mosnaim, D.; Nonhebel, D. C.; Russell, J. A. *Tetrahedron* **1969**, *25*, 3485. (b) Stewart, F. H. C. *Aust. J. Chem.* **1960**, *13*, 478. (c) Gimenez, R.; Pinol, M.; Serrano, L. *Chem. Mater.* **2004**, *16*, 1377.
- (16) Meech, S. R.; Phillips, D. J. *Photochem.* **1983**, *23*, 193.
- (17) Hanhela, P. J.; Paul, D. B. *Aus. J. Chem.* **1984**, *37*, 553.
- (18) Only strong electrostatic interaction between electrochemically generated di-ions of opposite charges leads to excimer emission with a characteristic broad and red-shifted emission in sterically hindered phenylanthracene-functionalized spirobifluorenes; see: Sartin, M.; Shu, C.; Bard, A. J. *J. Am. Chem. Soc.* **2008**, *130*, 5354.
- (19) The differences in the emission spectra for spin-coated and vacuum-deposited films point to differences in the molecular arrangements in the two films.

**Table 2.** EL Data for **1**, **2**, **4**, and **5** and the Model Compounds **8–10**

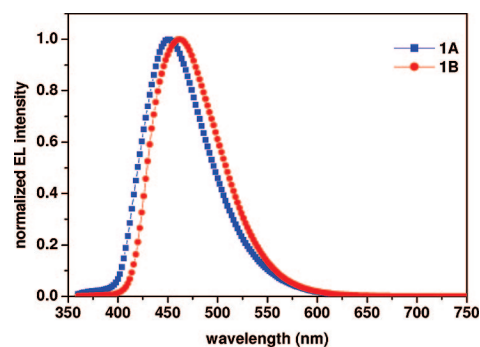
substrate <sup>a</sup>	$V_{on}$	$\eta_{ext}^b$	$\eta_p^b$	$\eta_l^b$	$\lambda_{max}^{EL}$	$L^b$ ( $V_d$ )	$L_{max}$	fwhm	CIE (x,y)
<b>1A</b>	4.5	1.17	0.48	1.24	452	248 (8.1)	4460	76	0.15, 0.13
		1.05 <sup>c</sup>	0.35 <sup>c</sup>	1.12 <sup>c</sup>		1117 <sup>c</sup> (10.1)			
<b>1B</b>	4.0	2.89	1.13	3.82	462	762 (10.6)	15303	78	0.15, 0.17
		1.42 <sup>c</sup>	0.77 <sup>c</sup>	3.20 <sup>c</sup>		3195 <sup>c</sup> (13.0)			
<b>2A</b>	3.5	0.28	0.31	0.64	498	129 (6.6)	3199	82	0.19, 0.38
		0.30 <sup>c</sup>	0.24 <sup>c</sup>	0.70 <sup>c</sup>		697 <sup>c</sup>			
<b>2B</b>	3.5	4.24	2.03	5.70	460	1139 (8.8)	13874	54	0.13, 0.18
		3.62 <sup>c</sup>	1.29 <sup>c</sup>	4.86 <sup>c</sup>		4853 <sup>c</sup> (11.8)			
<b>2C</b>	6.5	3.78	1.05	3.84	460	767 (11.5)	8200	48	0.12, 0.13
		2.86 <sup>c</sup>	0.65 <sup>c</sup>	2.91 <sup>c</sup>		2897 <sup>c</sup> (14.1)			
<b>4</b>	7.5	0.17 <sup>c</sup>	0.04 <sup>c</sup>	0.17 <sup>c</sup>	432	168 <sup>c</sup> (15.1)	332		0.18, 0.17
<b>5</b>	7.5	0.07 <sup>c</sup>	0.03 <sup>c</sup>	0.16 <sup>c</sup>	492	155 <sup>c</sup> (17.2)	227		0.20, 0.37
<b>8A</b>	5.5	0.17	0.09	0.29	454	59 (9.4)	831	84	0.20, 0.26
		0.17 <sup>c</sup>	0.08 <sup>c</sup>	0.28 <sup>c</sup>		279 <sup>c</sup> (11.4)			
<b>9A</b>	4.0	1.79	1.13	2.79	450	557 (7.8)	10992	108	0.17, 0.21
		1.57 <sup>c</sup>	0.84 <sup>c</sup>	2.45 <sup>c</sup>		2429 <sup>c</sup> (9.2)			
<b>9B</b>	3.5	2.82	1.01	2.54	452	508 (7.9)	8147	68	0.15, 0.10
		2.20 <sup>c</sup>	0.06 <sup>c</sup>	1.94 <sup>c</sup>		1944 <sup>c</sup> (9.8)			
<b>10A</b>	4.5	0.17	0.13	0.47	526	93 (11.7)	517	90	0.23, 0.44
		0.12 <sup>c</sup>	0.07 <sup>c</sup>	0.32 <sup>c</sup>		316 <sup>c</sup> (14.4)			

<sup>a</sup> **A**, **B**, and **C** refer to device configurations, which are (device **A**) ITO/NPB (400 Å)/**1** or **2** (100 Å)/TPBI (400 Å)/LiF (10 Å)/Al (1500 Å), (device **B**) ITO/NPB (400 Å)/**1** or **2**:MADN (400 Å)/TPBI (400 Å)/LiF (10 Å)/Al (1500 Å), and (device **C**) ITO/NPB (400 Å)/**1** or **2**:CBP (400 Å)/TPBI (400 Å)/LiF (10 Å)/Al (1500 Å). Those for **4** and **5** are ITO/PEDOT:PSS/5% **4**:PVK/TPBI (400 Å)/LiF (10 Å)/Al (1500 Å) and ITO/PEDOT:PSS/10% **5**:PVK/BCP (100 Å)/AIQ (300 Å)/LiF (10 Å)/Al (1500 Å). The films of **4** and **5** were prepared by spin-coating of solutions of **4** or **5** and PVK in chlorobenzene.  $V_{on}$  is the turn-on voltage,  $\eta_{ext}$  is the external quantum efficiency,  $\eta_p$  is the power efficiency (lm/W),  $\eta_l$  is the luminance efficiency (cd/A),  $L$  is the luminance (cd/m<sup>2</sup>),  $V_d$  is the driving voltage (V),  $L_{max}$  is the maximum luminance achieved (cd/m<sup>2</sup>), fwhm is the full width at half-maximum (nm), and CIE stands for 1931 Commission Internationale de l'Éclairage coordinates. <sup>b</sup> Measured at 20 mA/cm<sup>2</sup>. <sup>c</sup> Measured at 100 mA/cm<sup>2</sup>.

DSC experiments reveal that all compounds **1–7** possess stable thermal properties upon heating and cooling cycles; cf. the SI. Further, they exhibit high  $T_g$  values (Table 1). The X-ray powder diffraction profiles of anthracene-anchored bimesitylenes **4–7** show a lack of crystallinity when compared with their model analogue **8**; cf. the SI.

**Electrochemical Properties.** Cyclic voltammetric (CV) studies were performed to calculate the HOMO and LUMO values for **1–6**; the poor solubility of **7** precluded estimation of its HOMO by cyclic voltammetry. The CV experiments were carried out in solutions of 0.1 M supporting electrolyte (tetra-*n*-butylammonium hexafluorophosphate, TBAP) and 1 mM substrate in dry dichloromethane under an argon atmosphere using ferrocene as an internal standard. The representative voltammograms for **2**, **5**, and **6** are shown in Figure 2. The oxidation potential ( $E_{1/2}$ ) in each case was calculated by taking the average of the anodic and cathodic peak potentials. The values of the HOMOs for **1–6** thus calculated are 5.71 (**1**), 5.54 (**2**), 5.52 (**3**), 5.54 (**4**), 5.73 (**5**), and 5.69 (**6**) eV. From the HOMO values and the optical band gap energy available from the UV–vis spectra (Table 1), the energies of the LUMOs for **1–6** were calculated as follows: 2.76 (**1**), 2.83 (**2**), 3.05 (**3**), 2.56 (**4**), 3.04 (**5**), and 3.02 (**6**) eV.

**Electroluminescence Properties.** The functional behavior of the amorphous materials was examined typically for **1**, **2**, **4**, and **5** by constructing devices to capture electroluminescence. In our attempts, we discovered that the 2-fold functionalized anthracene derivatives **1** and **2** could be examined for electroluminescence by vacuum sublimation. Three types of multilayer devices, i.e., **A**, **B**, and **C**, were fabricated as follows: (device **A**) ITO/NPB (400 Å)/**1** or **2** (100 Å)/TPBI (400 Å)/LiF (10 Å)/Al (1500 Å); (device **B**) ITO/NPB (400 Å)/**1** or **2**:MADN (400 Å)/TPBI (400 Å)/LiF (10 Å)/Al (1500 Å); (device **C**) ITO/NPB (400 Å)/**1** or **2**:CBP (400 Å)/TPBI (400 Å)/LiF (10 Å)/Al (1500 Å). Indium–tin–oxide (ITO)-coated glass served as the anode, *N,N'*-bis(naphthalen-1-yl)-*N,N'*-bis(phenyl)benzidine (NPB) as a hole transporting layer, **1** or **2**

**Figure 3.** Electroluminescence spectra of **1** for two different devices, **A** and **B**.

as an emitter, 2-methyl-9,10-bis(naphthalen-2-yl)anthracene (MADN) and 4,4'-bis(carbazol-9-yl)biphenyl (CBP) as host emitting materials,<sup>23</sup> 2,2',2''-(1,3,5-benzenetriyl)tris(1-phenyl-1*H*-benzimidazole) (TPBI) as an electron transporting layer, and LiF:Al as the composite cathode. The performance characteristics (turn-on voltage, power efficiency, luminance efficiency, quantum efficiency, and CIE coordinates) of these devices are summarized in Table 2. As can be seen, both devices **A** and **B** for compound **1** exhibited a low turn-on voltage, bright luminance, and respectable external quantum efficiency. The doped device **B** showed better performance in comparison to that of the nondoped device **A** (Table 2). The EL spectra captured from the above devices of **1** are shown in Figure 3. In Figure 4 are shown the external efficiency vs current density plot and current–voltage–luminance profiles for both **1A** and **1B**.

The EL spectra recorded likewise for compound **2** under three different device configurations are shown in Figure 5. The spectra reveal blue and blue-green emissions according to the CIE

(20) Salbeck, J.; Yu, N.; Bauer, J.; Weissortel, F.; Bestgen, H. *Synth. Met.* **1997**, *91*, 209.

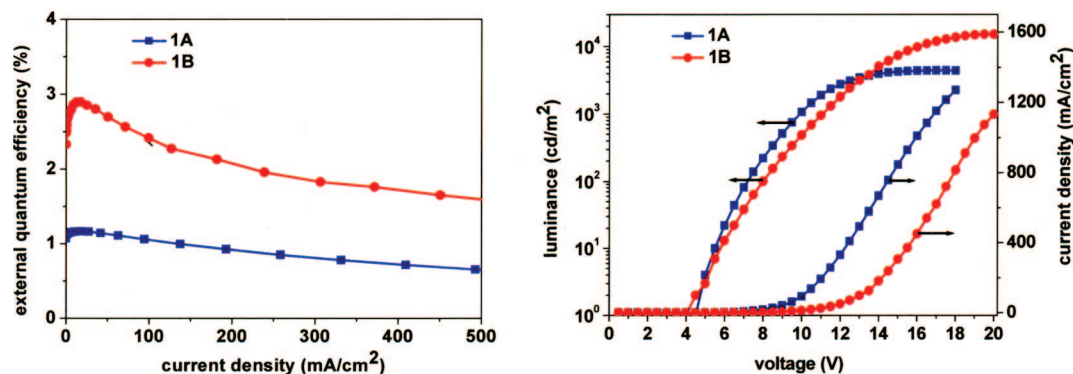


Figure 4. Device external quantum efficiency (left) and current–voltage–luminance (right) characteristics for **1A** and **1B**.

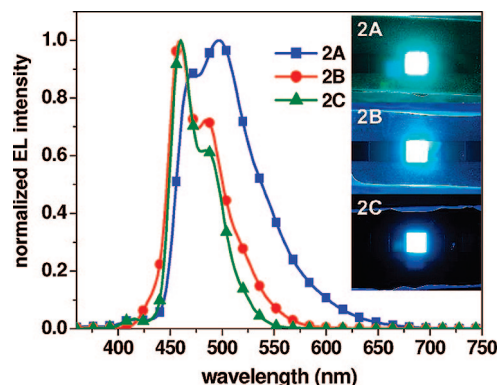


Figure 5. Electroluminescence spectra for **2** from three different devices, **A**, **B**, and **C**. The inset photographs show the blue-green to blue emitter from the devices of **2**.

chromaticity diagram. The current–voltage–luminance characteristics for nondoped and doped (1% **2**) devices are shown in Figure 6. For device **2C** with a CBP host, the current turns on at 3.5 V and the light later turns on at 6.5 V. The external quantum efficiency and brightness based on different types of fabrications are also shown in Figure 6. The doped devices **2B** and **2C** were found to be more efficient than the pure **2** device, that is, **2A**. As compared to the latter, a substantial increase in the efficiency from 0.28% to 4.24% was observed for device **2B** with a corresponding luminance enhancement from 129 to 1139 cd/m<sup>2</sup> at 20 mA/cm<sup>2</sup>. Figure 7 shows significantly improved peak EL efficiency, which increases from 3.84 cd/A or 1.05 lm/W (for **2C**) to 5.70 cd/A or 2.03 lm/W (for **2B**).

The 4-fold anthracene-functionalized bimesitylenes **4** and **5** could not be sublimed for construction of the devices via the vacuum-sublimation technique. Therefore, the fabrication was done by the spin-coating method. The doped device of configuration ITO/PEDOT:PSS/*x*% **4** or **5**:PVK/TPBI or BCP/Alq<sub>3</sub>/LiF/Al involving poly(vinylcarbazole) (PVK)<sup>24</sup> as the host improved the luminance and quantum efficiencies compared to the nondoped device. In the above configuration, PEDOT:PSS was the hole injection layer and a blend of PVK and compound **4** or **5** (*x*%, *x* = 5–25) that had been spun onto the hole injection layer from its solution in chlorobenzene served as the emitting layer. BCP (bathocuprine) was a hole-blocking layer, and TPBI or Alq<sub>3</sub> (tris(8-hydroxyquinoline)aluminum) served as an electron transporting layer. Finally, a composite cathode of LiF and Al was thermally evaporated onto the emitting layer sequentially. The performance characteristics of the above spin-

coated devices are collected in Table 2. The device for **5** emitted a blue-green light with  $\lambda_{\text{max}} = 492$  nm, and that for **4** emitted blue light with  $\lambda_{\text{max}} = 432$  nm. The EL spectra of **1**, **2**, **4**, and **5** from all the devices exhibit maxima closer to those observed in their PL (film) spectra.

For comparison, the electroluminescence of model compounds **8–10** was examined under doped (configuration **B**) as well as nondoped (configuration **A**) conditions. The performance results of the devices for **8–10** are collected in Table 2. In view of the best results noted above for compound **2** under doping conditions, the device performance characteristics of its model compound **9** were also examined under doping conditions. In Figure 8 are shown the EL spectra of **9** for nondoped (**A**) and doped (**B**) devices. The EL spectrum of device **9A** is characterized by a major band at ca. 450 nm followed by a low-energy band at ca. 510 nm, while the latter is conspicuously absent in that of **9B**. The origin of the long-wavelength band in device **9A** was probed by recording excitation and emission spectra for **9** in films of varying thickness; see the SI. The photoluminescence spectra showed that the intensity of the long-wavelength band increases relative to that of the major band at 450 nm with an increase (100–400 Å) in the thickness of the film. We attribute this feature to some kind of aggregation that manifests predominantly with increasing film thickness. Otherwise, it is noteworthy that the EL is captured with better efficiencies under doped conditions for this model compound as well; for example, the external efficiency is ca. 2.8% as compared to 1.8% under nondoped conditions; cf. Table 2.

## Discussion

As mentioned at the outset, there is a surge of interest in electroluminescence from organic molecules at the current time. Small-molecule-based OLEDs are considered more valuable than the polymer counterparts because of the difficulty in controlling the film thickness with polymers and the possibility of dissolution of the first layer during the coating of the second layer by spin-coating techniques. Further, the diversity of organic molecules with varying molecular weights and wide-ranging properties is simply unmatched by inorganic materials. Our design of EL materials constitutes a new category, which entails 2-fold/4-fold attachment of fluorophores to the basic extended-tetrahedral bimesitylene core by Suzuki/Sonogashira coupling protocols; the fluorophores, i.e., diphenylanthracene<sup>16</sup> and 9,10-bis(phenylethynyl)anthracene<sup>17</sup> in the present study, are so chosen as to exhibit, as a primary criterion, high fluorescence quantum yields in the solution state ( $\Phi_{\text{fl}} = \text{ca. } 0.9$ ). The motivations for consideration of anthracene derivatives were (i) they are well-known to undergo facile electrochemical

(21) Melhuish, W. H. *J. Phys. Chem.* **1961**, *65*, 229.

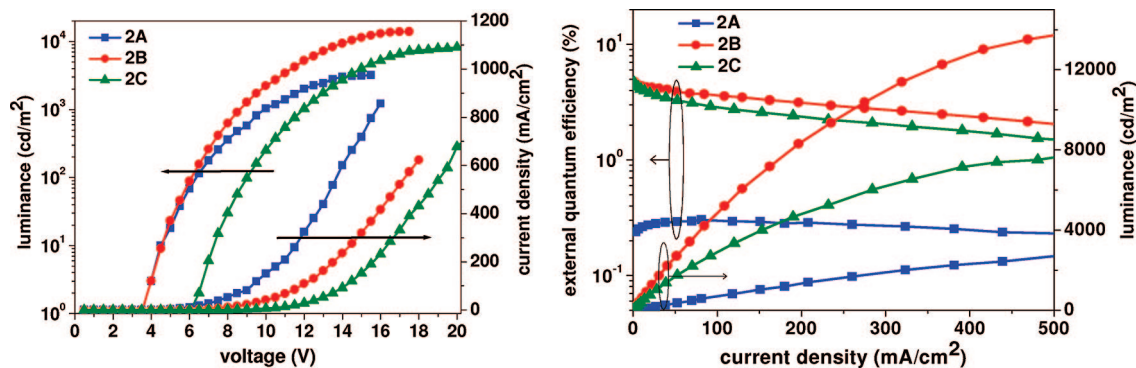


Figure 6. Current–voltage–luminance (left) and efficiency–luminance–current (right) characteristics for the different 2 devices, i.e., 2A, 2B, and 2c.

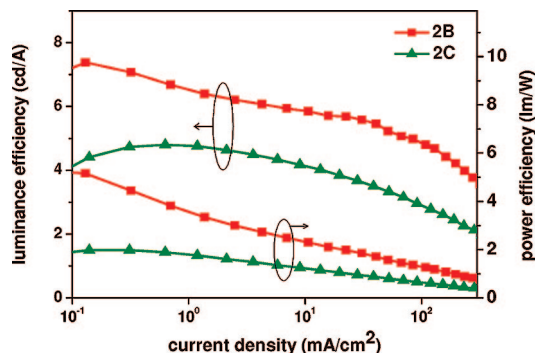


Figure 7. Luminance and power efficiencies for 2 under doping conditions with device configurations B and C.

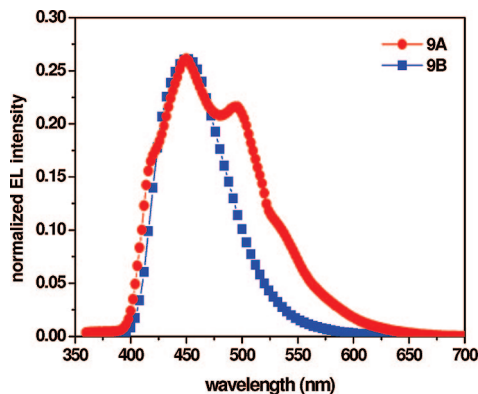


Figure 8. Electroluminescence spectra of 9,10-diphenylanthracene (9) under nondoped (A) and doped (B) conditions.

oxidation (hole transporting) and reduction (electron transporting) reactions<sup>25</sup> and hence have found use in electroluminescent devices and (ii) there is a continued interest in exploiting them for electroluminescence since the discovery of electrolumines-

cence in anthracene crystals<sup>26</sup> due to their blue emission, which is crucial for development of OLEDs with white emission, vide infra.

As shown in Scheme 1, the synthesis of a number of anthracene derivatives is readily accomplished via Pd(0)-mediated Suzuki and Sonogashira coupling reactions. The unique advantage is 2-fold or 4-fold functionalization of the bimesitylene selectively, which is rather tedious for spirobifluorene and heretofore unknown for tetraphenylmethane.<sup>27</sup> That the 3-dimensional molecular topology of 1–7 does indeed manifest in the amorphous nature is clearly revealed from their powder X-ray diffraction patterns (cf. the SI). The thermal stability is an important property for a molecule to be used in a device.<sup>28</sup> Several strategies and methods have been explored to achieve high thermal stabilities. The anthracene-anchored bimesityls were isolated as highly amorphous ( $T_g \approx 190$ – $330$  °C) compounds with a high thermal stability (decomposition starts above 420 °C); for example, the  $T_d$  values for 2-fold and 4-fold functionalized bimesitylenes 1 and 4 are 470–520 °C as compared to 260 °C for its model monomeric compound 9. The DSC analyses for 1–7 show that the  $T_g$  values increase with an increase in the rigidity and bulkiness (Table 1). Thus, the extended-tetrahedral geometry, the rigidity extant to the bimesitylene core, and 2-fold/4-fold substitution with large and bulky substituents such as anthracenes manifest not only in high glass transition ( $T_g$ ) temperatures, but also in thermal decomposition ( $T_d$ ) temperatures.

As shown in Figure 1, 1–7 exhibit UV–vis absorption profiles that are characteristic of anthracene. It is noteworthy that the absorption maximum shifts toward the longer wavelength region by ca. 30–40 nm upon introduction of an additional triple bond as we go from 4 and 5 to 6 and 7. Replacement of ethyne by a phenyl ring results in a blue shift (1 and 3, Table 1), evidently due to the break in conjugation, since the aryl rings attached to the core remain perpendicular.<sup>7c</sup> The optical band gap energy values ( $E_g^{opt}$ ) calculated from the tail end of the absorption vary from 2.46 to 2.98 eV (see Table 1).

All compounds 1–7 exhibit very high emission intensities at concentrations as low as  $10^{-5}$ – $10^{-6}$  M. The effect of an

(22) When the films were subjected to heat treatment (annealing) under vacuum, the emission intensity of the films was found to decrease considerably by 2–3-fold with a broadening in their spectral profiles. Presumably, the annealing leads to some kind of reorganization of the molecules within the amorphous film in a way that the emission is suppressed. That the thermal heating does not lead to recrystallization was established from powder XRD of the bimesitylenes 1 and 5 before and after annealing; cf. the SI.

(23) For use of MADN as a dopant, see: (a) Lee, M. T.; Chen, H. H.; Liao, C. H.; Tsai, C. H.; Chen, C. H. *Appl. Phys. Lett.* **2004**, *85*, 3301. (b) Lee, M. T.; Liao, C. H.; Tsai, C. H.; Chen, C. H. *Adv. Mater.* **2005**, *17*, 2493.

(24) For use of PVK as a host, see: Robinson, M. R.; Wang, S.; Bazan, G. C.; Cao, Y. *Adv. Mater.* **2000**, *12*, 1701.

(25) (a) Kim, Y. H.; Kwon, S. K.; Yoo, D. S.; Rubner, M. F.; Wrighton, M. S. *Chem. Mater.* **1997**, *9*, 2699. (b) Shi, J.; Tang, C. W. *Appl. Phys. Lett.* **2002**, *80*, 3201. (c) Benzman, R.; Faulkner, L. R. *J. Am. Chem. Soc.* **1972**, *94*, 6317. (d) Garay, R. O.; Naarmann, H.; Müllen, K. *Macromolecules* **1994**, *27*, 1922. (e) Shih, H. T.; Lin, C. H.; Shih, H. H.; Cheng, C. H. *Adv. Mater.* **2002**, *14*, 1409. (f) Danel, K.; Hwang, T. H.; Lin, J. T.; Tao, Y. T.; Chen, C. H. *Chem. Mater.* **2002**, *14*, 3860. (g) Yu, M. X.; Duan, J. P.; Lin, C. H.; Chung, C. H.; Tao, Y. T. *Chem. Mater.* **2002**, *14*, 3948.

increase in conjugation is clearly revealed in the emission maxima, which vary from ca. 450 to 570 nm (blue to blue-green to green). Thus, the emission properties can be modulated by appropriate structural modifications. Further, the films do not appear to reveal any aggregation behavior at least for **1**, **2**, and **4–6**. What is noteworthy is the conservation of photo-physical properties of the constituent fluorophores, i.e., anthracenes, upon 4-fold functionalization, which further attests to the fact that the conjugation is only weakly transmitted in the *meta* linkage. The fluorescence quantum efficiencies of all **1–7** are quite high (Table 1) and vary from 0.55 to 0.86. It should be noted that the attachment of the small molecular fluorophores to the bimesityl core leading to branched systems results only in marginal variations in the quantum yields as compared to those of the free constituent fluorophores **8–10**.

The functional behavior of the branched amorphous systems **1–7** was demonstrated by capturing electroluminescence for **1**, **2**, **4**, and **5** as representative cases. In general, the devices based on anthracenes are renowned for their excellent stability.<sup>23a</sup> For 2-fold anthracene-functionalized bimesitylenes **1** and **2**, the OLEDs of two configurations, **A** (nondoped) and **B** (doped), were fabricated by vacuum deposition. The host material in the emitting layer of device **C** is CBP, while that in device **B** is MADN. The results of devices summarized in Table 2 for bimesitylenes **1** and **2** as well as for the model compounds **8–10** suggest that the performance characteristics under nondoped conditions (**A**) are unexceptional. Otherwise, it is pertinent to note that the EL spectrum of nondoped 2-fold functionalized anthracene **1**, i.e., **1A** (Figure 3), reveals the absence of the long-wavelength emission at ca. 500 nm, which is prominently observed in the EL of its model compound **9**; see **9A**, Figure 8. Given that the long-wavelength emission presumably owes its origin to aggregation as mentioned earlier, its absence in **1A** clearly attests to the advantage of the bimesitylene scaffold in obviating such a manifestation of long-wavelength emission.

In contrast to the nondoped devices, the doped devices (**B** and **C**) for **1** and **2** as well as for the model compound **9** can be turned on between 3.5 and 6.5 V with intensities in the range of 508–1140 cd/m<sup>2</sup> at a current density of 20 mA/cm<sup>2</sup>. Further, the external quantum efficiency increases by 2.5 times for **1B** as compared to that for **1A**; the efficiency increases from 1.17% to 2.89% and the luminescence efficiency from 248 to 762 cd/m<sup>2</sup>. Device **1B** shows a maximum luminance of ~15 300 cd/m<sup>2</sup> with CIE<sub>x,y</sub> ( $x = 0.15, y = 0.17$ ). Clearly, the energy transfer from the MADN host to the **1** dopant is efficient.<sup>29</sup> The EL spectrum for device **2A** shows a major peak at 498 nm and a shoulder at 470 nm with an fwhm of 82 nm, Figure 5. While both of the doped devices **2B** and **2C** exhibit a major peak at 460 nm and a shoulder at 484 nm, the fwhm decreases to 54 nm for the MADN host device (**2B**) and 48 nm for the CBP host device (**2C**). The delay in the light emission turn-on for **2C** suggests that the hole and electron carriers are not properly balanced. The energy diagram for the two device configurations **B** and **C** of compound **2** is shown in Figure 9. Due to the mismatch in the LUMO levels of CBP and TPBI by 0.6 eV, the electron injection is presumably more difficult than the hole

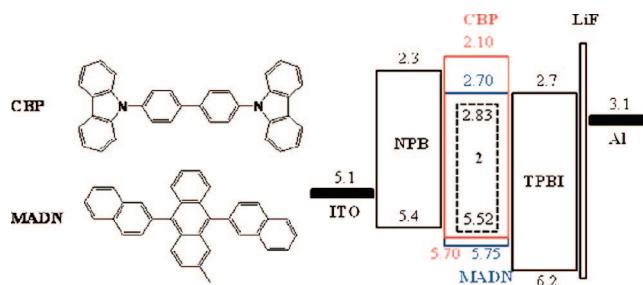


**Figure 9.** Energy diagram for the devices doped with anthracene-functionalized bimesitylenes. Also shown are the molecular structures of CBP and MADN, which are employed as host emitting materials.

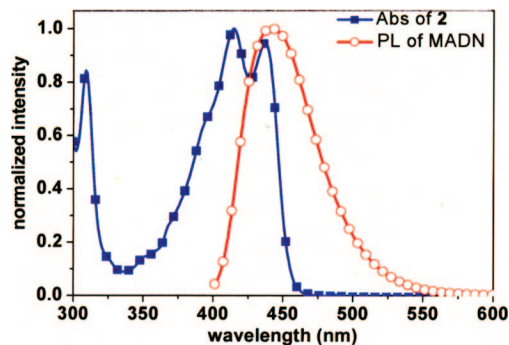


**Figure 10.** Absorption spectrum of **2** and photoluminescence spectrum of MADN.

injection in device **2C**. However, for MADN as the host, both the current and light turn-on voltages occurred at 3.5 V. This suggests that hole and electron carriers are perfectly balanced to facilitate easy electron injection compared to the case when the host used was CBP, which is evidently due to the energy gap between the LUMO levels of MADN and TPBI being very negligible. Further, the peak EL efficiency increases from 3.84 cd/A for **2C** to 5.70 cd/A for **2B**. Relatively poor efficiency in the case of **2C** is also presumably due to the possibility that the high concentration of planar CBP host leads to crystallization in the emitting layer film. For the devices with MADN as the host and anthracene derivatives as blue-fluorescent guests, the reduction in driving voltages, compared to the case when CBP was used as the host, should be traceable to a narrower HOMO–LUMO energy gap for MADN than for CBP. In other words, the HOMO and LUMO energy levels of **2** lie well within those of the host MADN (HOMO = 5.75 eV, LUMO = 2.70 eV) for Förster-type energy transfer to occur efficiently. Indeed, the absorption spectrum of **2** exhibits a good overlap with the emission spectrum of MADN (Figure 10). Among all the devices, device **2B** shows the highest luminance of ~13 900 cd/m<sup>2</sup> at 17.5 V, maximum luminance efficiency of ~7.4 cd/A at 4.5 V, and power efficiency of ~5.3 lm/W at 4.0 V. Further, at a brightness of 800 cd/m<sup>2</sup> and a current density of 13.8 mA/cm<sup>2</sup>, device **2B** exhibits an excellent luminance efficiency of 5.8 cd/A, an external quantum efficiency of 4.3% with a power efficiency of 2.2 lm/W, and pure blue light with a CIE<sub>x,y</sub> ( $x = 0.13, y = 0.18$ ). The morphological stability of all the devices based on the bimesityl scaffold was found to be excellent. Besides, the results with doping are comparable to or better than those reported thus far for anthracene-based organic light emitting diodes.<sup>30</sup>

(26) Tang, C. W.; Van Slyke, S. A. *Appl. Phys. Lett.* **1987**, *51*, 913.

(27) (a) Chiang, C. L.; Shu, C. F.; Chen, C. T. *Org. Lett.* **2005**, *7*, 3717. For a very recent synthesis and electroluminescence study on 2-fold anthracene-functionalized tetraarylsilicon, see: (b) Lyu, Y.-Y.; Kwak, J.; Lee, S.-H.; Kim, D.; Lee, C.; Char, K. *Adv. Mater.* **2008**, *20*, 2720.

(28) Tokito, S.; Tanaka, H.; Noda, K.; Okada, A.; Taga, T. *Appl. Phys. Lett.* **1997**, *70*, 1929.

(29) Pope, M.; Swenberg, C. E. *Electronic Processes on Organic Crystals*; Clarendon: Oxford, 1982.

In contrast, the spin-coated devices made from the blend of PVK and **4/5** were rather unsatisfactory. Although the EL spectra of **4** and **5** are similar to their PL spectra, the significantly low emission from PVK appears unavoidable due to the device structures even with high doping concentrations (ca. 25%). Further, the emission from TPBI—the electron transporting/hole blocking layer—in the TPBI-based devices suggests that some proportion of holes are transported very fast through the emitting layer and recombine in the TPBI layer, leading to TPBI emission. The change of solvent from chlorobenzene to toluene for spin-coating does improve the efficiency by 2-fold, while solvents such as THF, 1,2-dichloroethane, etc. do not produce good-quality films. The comparative EL spectra of the Alq3- and TPBI-based devices with varying doping concentrations are collected in the Supporting Information. The poor device efficiency in these fabricated devices may be attributed to poor film morphology and rapid charge neutralization at the electrodes via a self-quenching mechanism leading to poor recombination. Clearly, more experimentation with the device fabrication via spin-coating techniques is necessary to further delineate the potential of this new class of 4-fold functionalized amorphous materials. Otherwise, the efficient functional behavior as OLEDs for the molecules that can be sublimed is amply demonstrated from the results observed for **1** and **2**.

Given that electroluminescence closely follows the trend observed for photoluminescence from films or in the solution state (under conditions that the emission is not observed from dopants), the anthracene-functionalized bimesityls **1–7** constitute an excellent series with blue and blue-green emission properties with associated wide optical band gaps. Indeed, the host emitters with wide band gap energies are of great importance, as they can be used to dope the red emitting materials with narrow band gap energies to elicit white light emission.<sup>31</sup> This, indeed, is the cause for a surge of interest in blue light emitting materials. Several groups have achieved white light emission from such wide band gap materials via downhill energy transfer.<sup>32</sup> White light emission is considered vital, as all the colors can be derived from it to produce a full color display.

## Conclusions

We have shown that the molecular scaffolds based on a  $D_{2d}$ -symmetric 3-dimensional bimesityl core can be exploited to design rigid and high molecular weight 2- and 4-fold fluorophore-functionalized derivatives. While a variety of design strategies have been reported so far, the anthracene-function-

alized bimesityls **1–7** correspond to a new and unique category. It is shown that **1–7** can be readily synthesized via Pd(0)-mediated Suzuki and Sonogashira protocols. While the rigidity and 3-dimensional topology seemingly render the molecular packing difficult, leading to an amorphous nature, the high molecular weight in conjunction with anthracene fluorophores that are linked to bimesityl appears to contribute to  $T_g$  values as high as ca. 300 °C. Further advantages of the design are (i) the emission wavelength can be modulated with a suitable choice of the fluorophore and (ii) the fluorescence quantum yields of the constituent fluorophores are reliably reproduced upon 2- or 4-fold functionalization. That the molecular attributes, which are pivotal to predicting efficient molecular packing and failure thereof, manifest in amorphous properties for application in OLEDs with high  $T_g$  and  $T_d$  values is demonstrated by fabrication of OLED devices; the 2-fold functionalized derivatives **1** and **2** lend themselves to sublimation techniques, so that the electroluminescence is captured with high efficiencies at low turn-on voltages. The performance characteristics of the devices fabricated for **1** and **2** are far more superior to those reported so far for the anthracene-based OLEDs. Although the 4-fold functionalized systems did not permit sublimation, leading to spin-coating as a means for device fabrication, the observed electroluminescence for **4** and **5** attests to a broader scope and applicability of this new category of amorphous molecules for application in OLEDs.

## Experimental Section

**General Aspects.** All the palladium-mediated cross-coupling reactions were performed under a nitrogen gas atmosphere in oven-dried pressure tubes.  $^1\text{H}$  and  $^{13}\text{C}$  NMR spectra were recorded on a JEOL (400 MHz) or Bruker (300/400/500 MHz) spectrometer in  $\text{CDCl}_3$  as a solvent. Chemical shifts are reported in  $\delta$  scale downfield from the peak for tetramethylsilane. The FAB mass spectra were recorded on a JEOL SX-102/mass system using argon/xenon as the FAB gas in the linear mode with *m*-nitrobenzyl alcohol as the matrix. The PXRD results were recorded using a Seifert powder X-ray diffractometer with  $\text{Cu K}\alpha$  ( $\lambda = 1.54056 \text{ \AA}$ ) radiation. The TGA and DSC measurements were carried out with a heating rate of 10 °C/min under a nitrogen or argon gas atmosphere. UV–vis absorption spectra were recorded using a Jasco-550 spectrophotometer. Photoluminescence spectra and PL quantum yields were obtained from a Spex Fluorolog-2/Hitachi F-4500 spectrofluorimeter. The photoluminescence spectra of solutions were measured in spectral grade solvents using a 90° angle of detection, and those of the thin solid films were measured by front-face detection. The current–voltage ( $I$ – $V$ ) characteristics were recorded by a Keithley model 2400 electrometer. The Commission Internationale de l’Eclairage (CIE) coordinates of the devices were measured by a PR650 spectroscan spectrometer. All measurements were carried out at ambient conditions.

Dry tetrahydrofuran (THF) and toluene were freshly distilled over sodium prior to use. Triethylamine and diisopropylamine were distilled from KOH. All the reactions were monitored by analytical thin layer chromatography (TLC) using commercial aluminum sheets precoated with silica gel. Chromatography was conducted on silica gel (Acme, Mumbai, 60–120 mesh). All commercial chemicals were used as received.

The starting materials, viz., bimesityl<sup>6c</sup> and **11**,<sup>6c</sup> were synthesized according to the earlier reported procedures established from our laboratories.<sup>6</sup> **15**,<sup>13a,b</sup> **16**,<sup>13a,b</sup> and **17**<sup>13</sup> were prepared according to the literature procedures.<sup>13</sup>

**Preparation of 3,3'-Diiodobimesityl.** In a two-necked round-bottom flask, bimesityl (0.40 g, 1.68 mmol) was dissolved in 8 mL of  $\text{CH}_3\text{CN}$ . To this was added 0.83 g (3.69 mmol) of NIS followed by 0.08 mL of TFA (catalytic amount) under vigorous stirring and cold conditions. The reaction mixture was allowed to

- (30) (a) Shen, W.-J.; Dodda, R.; Wu, C.-C.; Wu, F.-I.; Liu, T.-H.; Chen, H.-H.; Chen, C. H.; Shu, C.-F. *Chem. Mater.* **2004**, *16*, 930. (b) Kim, Y.-H.; Shin, D.-C.; Kim, S.-H.; Ko, C.-H.; Yu, H.-S.; Chae, Y.-S.; Kwon, S.-K. *Adv. Mater.* **2001**, *13*, 1690. (c) Benmansour, H.; Shioya, T.; Sato, Y.; Bazan, G. C. *Adv. Funct. Mater.* **2003**, *13*, 883. (d) Shih, P.-I.; Chuang, C.-Y.; Chien, C.-H.; Diau, E. W.-G.; Shu, C.-F. *Adv. Funct. Mater.* **2007**, *17*, 3141. (e) Kim, Y.-H.; Jeong, H.-C.; Kim, S.-H.; Yang, K.; Kwon, S.-K. *Adv. Funct. Mater.* **2005**, *15*, 1799. (f) Lee, M.-T.; Liao, C.-H.; Tsai, C.-H.; Chen, C. H. *Adv. Mater.* **2005**, *17*, 2493. (g) Zhang, X. H.; Liu, M. W.; Wong, O. Y.; Lee, C. S.; Kwong, H. L.; Lee, S. T.; Wu, S. K. *Chem. Phys. Lett.* **2003**, *369*, 478. (h) Tao, S. L.; Hong, Z. R.; Peng, Z. K.; Ju, W. G.; Zhang, X. H.; Wang, P. F.; Wu, S. K.; Lee, S. T. *Chem. Phys. Lett.* **2004**, *397*, 1. (i) Shi, J.; Tang, C. W. *Appl. Phys. Lett.* **2002**, *80*, 3201. (j) Kan, Y.; Wang, L.; Duan, L.; Hu, Y.; Wu, G.; Qiu, Y. *Appl. Phys. Lett.* **2004**, *84*, 1513. (k) Li, H.-C.; Lin, Y.-P.; Chou, P.-T.; Cheng, Y.-M.; Liu, R.-S. *Adv. Funct. Mater.* **2007**, *17*, 520.
- (31) (a) Zhang, X. H.; Liu, M. W.; Wong, O. Y.; Lee, C. S.; Kwong, H. L.; Lee, S. T.; Wu, S. K. *Chem. Phys. Lett.* **2003**, *369*, 478. (b) Cheon, K. O.; Shinar, J. *Appl. Phys. Lett.* **2002**, *81*, 1738.

stir for 8 h. Subsequently, the reaction mixture was concentrated, and the organic matter was extracted with  $\text{CHCl}_3$ . The combined extract was washed with  $\text{NaHCO}_3$  solution followed by brine, dried over anhydrous  $\text{Na}_2\text{SO}_4$ , filtered, and evaporated to dryness. Careful silica gel column chromatography using  $\text{CHCl}_3$  and petroleum ether afforded the colorless diiodobimesityl (0.68 g) in 83% yield: IR (KBr,  $\text{cm}^{-1}$ ) 2970, 2947, 2915, 1449, 1375;  $^1\text{H}$  NMR ( $\text{CDCl}_3$ , 400 MHz)  $\delta$  1.78 (s, 6H), 2.07 (s, 6H), 2.48 (s, 6H), 7.03 (s, 2H);  $^{13}\text{C}$  NMR ( $\text{CDCl}_3$ , 100 MHz)  $\delta$  19.6, 26.7, 29.9, 106.2, 129.0, 135.2, 138.3, 138.8, 140.7.

**Preparation of 3,3',5,5'-Tetrakis[(trimethylsilyl)ethynyl]bimesityl.** An oven-dried pressure tube was cooled under nitrogen gas and charged with  $\text{Pd}(\text{PPh}_3)_4$  (0.078 g, 0.06 mmol),  $\text{CuI}$  (0.0065 g, 0.03 mmol), **11** (0.50 g, 0.67 mmol), (trimethylsilyl)acetylene (0.33 g, 3.36 mmol), and  $\text{Et}_3\text{N}$  (12.5 mL). Subsequently, the tube was sealed, and the mixture was heated at 90 °C for 36 h. After the usual workup, a short pad filtration was performed to obtain the compound as a pure material (0.41 g, 97%):  $^1\text{H}$  NMR (400 MHz,  $\text{CDCl}_3$ )  $\delta$  0.26 (s, 36H), 1.99 (s, 12H), 2.63 (s, 6H);  $^{13}\text{C}$  NMR (100 MHz,  $\text{CDCl}_3$ )  $\delta$  0.10, 18.6, 20.0, 102.5, 102.9, 121.4, 137.0, 138.5, 142.3.

**Preparation of 3,3'-Bis[(trimethylsilyl)ethynyl]bimesityl.** This compound was prepared by following the procedure described above. Diiodobimesitylene and 4 equiv of (trimethylsilyl)acetylene were used as coupling agents, and  $\text{Pd}(\text{PPh}_3)_4$  (10 mol %) was used as the catalyst. The desired compound was obtained in a yield of 99%:  $^1\text{H}$  NMR (300 MHz,  $\text{CDCl}_3$ )  $\delta$  0.24 (s, 18H), 1.79 (s, 6H), 1.97 (s, 6H), 2.43 (s, 6H), 6.95 (s, 6H);  $^{13}\text{C}$  NMR (100 MHz,  $\text{CDCl}_3$ )  $\delta$  0.19, 18.1, 20.1, 21.0, 102.0, 103.5, 120.9, 128.6, 136.1, 137.0, 138.2, 139.4.

**Preparation of 3,3',5,5'-Tetraethynylbimesityl, 12.** Desilylation was carried out by adding  $n\text{-Bu}_4\text{NF}$  (3.15 mL of a 1 M solution in THF) dropwise at 0 °C to a solution of tetrakis[(trimethylsilyl)ethynyl]bimesityl (0.41 g, 0.65 mmol) in 10 mL of dry THF under a nitrogen atmosphere. The reaction mixture was slowly allowed to attain room temperature, and the mixture was stirred for a further 6 h. The solvent was removed in vacuo, and the residue was poured into water and extracted with dichloromethane. The organic matter thus obtained was subjected to rapid column chromatography on silica gel to obtain the pure product (0.21 g, 97%):  $^1\text{H}$  NMR (400 MHz,  $\text{CDCl}_3$ )  $\delta$  1.98 (s, 12H), 2.65 (s, 6H), 3.50 (s, 4H);  $^{13}\text{C}$  NMR (100 MHz,  $\text{CDCl}_3$ )  $\delta$  18.6, 19.9, 76.6, 77.0, 77.3, 81.2, 85.3, 120.6, 137.0, 139.0, 142.9.

**Preparation of 3,3'-Diethynylbimesityl.** This compound was prepared starting from 3,3'-bis[(trimethylsilyl)ethynyl]bimesityl by following the procedure described above (yield 96%):  $^1\text{H}$  NMR (400 MHz,  $\text{CDCl}_3$ )  $\delta$  1.82 (s, 6H), 1.99 (s, 6H), 2.45 (s, 6H), 3.47 (s, 2H), 6.98 (s, 2H);  $^{13}\text{C}$  NMR (100 MHz,  $\text{CDCl}_3$ )  $\delta$  18.1, 20.1, 20.9, 81.9, 84.8, 119.9, 128.7, 136.3, 137.0, 138.5, 139.6.

**Synthesis of 1.** Diiodobimesityl (0.627 g, 1.28 mmol), 9-(4-bromophenyl)-10-phenylanthraceneboronic acid (**14**) (1.40 g, 3.74 mmol), and  $\text{Pd}(\text{PPh}_3)_4$  (0.118 g, 8 mol %) were introduced into an initially oven-dried pressure tube under  $\text{N}_2$  gas. To this mixture were added dry toluene (10 mL), dry THF (5 mL), and 2 M  $\text{K}_2\text{CO}_3$  solution (5 mL). The reaction mixture was heated slowly from 70 to 110 °C and maintained at this temperature for 36 h with constant stirring. After this period, the reaction mixture was cooled and the contents were extracted with  $\text{CHCl}_3$ . Careful column chromatography over silica gel with 10–25% dichloromethane in petroleum ether followed by purification via precipitation of the compound from its solution in chloroform by adding methanol led to 0.45 g (41%) of **1** as a colorless solid material:  $^1\text{H}$  NMR (500 MHz,  $\text{CDCl}_3$ )  $\delta$  1.89 (s, 6H), 2.07 (s, 6H), 2.29 (s, 6H), 7.19 (s, 2H), 7.30–7.45 (m, 10H), 7.46–7.67 (m, 16H), 7.69–7.86 (m, 8H);  $^{13}\text{C}$  NMR (125 MHz,  $\text{CDCl}_3$ )  $\delta$  18.2, 20.1, 21.2, 125.0, 127.0, 127.4, 128.4, 128.9, 129.5, 129.9, 130.0, 131.2, 131.3, 133.7, 134.3, 134.5, 136.9, 137.0, 137.2, 138.3, 139.1, 139.8, 141.1; FAB-MS  $m/z$  894

( $\text{M}^+$ ); HRMS  $m/z$  calcd for  $\text{C}_{70}\text{H}_{54}$  894.4226, found 894.4209 ( $\text{M}^+$ ). Anal. Calcd for  $\text{C}_{70}\text{H}_{54}$ : C, 93.92; H, 6.08. Found: C, 93.93; H, 5.71.

**General Procedure for the Synthesis of Tetraphenylbimesityl via 4-Fold Suzuki Coupling.** The following is a representative procedure for 4-fold Suzuki coupling.

**Preparation of 3,3',5,5'-Tetraphenylbimesityl, 11** (2.22 g, 3.0 mmol), phenylboronic acid (2.90 g, 24.0 mmol), and  $\text{Pd}(\text{PPh}_3)_4$  (0.69 g, 20 mol %) were introduced into an initially oven-dried pressure tube under  $\text{N}_2$ . To this mixture were added dry toluene (15 mL) and saturated  $\text{NaHCO}_3$  solution (15 mL). The reaction mixture was heated slowly from 80 to 120 °C and maintained at the latter for 12 h with constant stirring. After this period, the reaction mixture was cooled, and the contents were extracted with  $\text{CHCl}_3$ . Silica gel column chromatography using 5% chloroform in hexane yielded 1.25 g (77%) of tetraphenylbimesityl as a colorless solid material: IR (KBr,  $\text{cm}^{-1}$ ) 3020, 2921, 1598, 1492, 1438;  $^1\text{H}$  NMR (400 MHz,  $\text{CDCl}_3$ )  $\delta$  1.71 (s, 12H), 1.72 (s, 6H), 7.23 (m, 8H), 7.32 (m, 4H), 7.42 (m, 8H);  $^{13}\text{C}$  NMR (100 MHz,  $\text{CDCl}_3$ )  $\delta$  18.3, 19.3, 126.2, 128.2, 129.5, 131.9, 132.4, 138.7, 140.0, 142.5.

**Preparation of 3,3',5,5'-Tetrakis(4-bromophenyl)bimesityl.** A solution of tetraphenylbimesityl (1.25 g, 2.3 mmol) in  $\text{CHCl}_3$  was treated, under constant stirring and in the presence of Fe powder (0.2 mmol) as a catalyst, with liquid bromine (0.5 mL, 9.66 mmol) and stirred at room temperature for 4 h. After this period, it was diluted with  $\text{CHCl}_3$ , washed well with 2 N  $\text{NaOH}$  solution, and dried over anhydrous  $\text{Na}_2\text{SO}_4$ . After removal of the solvent under vacuum, the crude product was recrystallized from  $\text{EtOAc}$ , yield 1.68 g (86%), colorless solid: IR (KBr,  $\text{cm}^{-1}$ ) 2921, 2855, 1487, 1445, 1386;  $^1\text{H}$  NMR (400 MHz,  $\text{CDCl}_3$ )  $\delta$  1.63 (s, 12H), 1.67 (s, 6H), 7.06 (d,  $J = 8.3$  Hz, 8H), 7.54 (d,  $J = 8.3$  Hz, 8H);  $^{13}\text{C}$  NMR (100 MHz,  $\text{CDCl}_3$ )  $\delta$  18.2, 19.3, 120.5, 131.2, 131.6, 132.0, 132.6, 138.5, 139.0, 140.9.

**Preparation of Tetraboronate Ester 13.** A solution of tetrakis(4-bromophenyl)bimesityl (0.60 g, 0.69 mmol) in dry THF (40 mL) was cooled to  $-78$  °C. A 1.6 M solution of  $n\text{-BuLi}$  in hexanes (2.6 mL, 4.19 mmol) was introduced slowly dropwise into the above well-stirred solution. The reaction mixture turned red-brown in color. It was allowed to stir for a further 15–20 min, and triisopropyl borate (1.9 mL, 8.38 mmol) was slowly introduced. Subsequently, the reaction mixture was stirred for 30 min at the same temperature and allowed to warm to room temperature over a period of 5 h. The solvent was removed under reduced pressure and dried thoroughly to obtain a pale yellow solid. The isopropyl boronate ester was dissolved in dry toluene (150 mL), and pinacol (1.35 g, 11.4 mmol) was introduced. The contents were heated at reflux overnight with a Dean–Stark apparatus. At the end of the reaction, the reaction mixture was concentrated, and the organic matter was extracted with  $\text{CHCl}_3$ . The organic layer was washed with brine, dried over anhydrous  $\text{Na}_2\text{SO}_4$ , filtered, and evaporated to yield a crude product. Rapid column chromatography using 25%  $\text{EtOAc}$  in petroleum ether afforded pure boronate ester as a colorless solid, yield 0.84 g (86%): IR (KBr,  $\text{cm}^{-1}$ ) 2978, 2927, 1609, 1447, 1396;  $^1\text{H}$  NMR (400 MHz,  $\text{CDCl}_3$ )  $\delta$  1.36 (s, 48H), 1.64 (s, 6H), 1.66 (s, 12H), 7.23 (d,  $J = 8.0$  Hz, 8H), 7.87 (d,  $J = 8.0$  Hz, 8H);  $^{13}\text{C}$  NMR (100 MHz,  $\text{CDCl}_3$ )  $\delta$  18.3, 19.3, 24.9, 83.7, 129.0, 131.6, 132.2, 134.8, 138.6, 140.0, 145.6.

**Synthesis of 4.** To an oven-dried pressure tube cooled under  $\text{N}_2$  were added tetraboronate ester **13** (0.104 g, 0.10 mmol), **15** (0.26 g, 0.79 mmol),  $\text{Pd}(\text{PPh}_3)_4$  (0.009 g, 10 mol %), dry toluene (4.0 mL), and 2 M  $\text{Na}_2\text{CO}_3$  (2.0 mL). The solution was purged thoroughly with nitrogen gas, the tube sealed tightly, and the solution heated at 110 °C. A pale brown solid began to form after 10 h. After 24 h, the reaction mixture was worked up in the usual manner. The residue was purified by silica gel column chromatography using chloroform–petroleum ether as the eluent. The product obtained was further purified by precipitation from  $\text{CHCl}_3$  solution using petroleum ether/methanol, which led to isolation of the pure

product (0.15 g, 52%) as a colorless powder: IR (KBr,  $\text{cm}^{-1}$ ) 2920, 1603, 1442, 1388, 1022;  $^1\text{H}$  NMR (500 MHz,  $\text{CDCl}_3$ )  $\delta$  2.09 (s, 12H), 2.3 (s, 6H), 7.32–7.40 (m, 16H), 7.46–7.48 (m, 8H), 7.55–7.62 (m, 28H), 7.65–7.73 (m, 8H), 7.75 (t,  $J = 5.0$  Hz, 8H);  $^{13}\text{C}$  NMR (125 MHz,  $\text{CDCl}_3$ )  $\delta$  18.8, 20.0, 125.0, 127.0, 127.4, 128.4, 129.7, 129.9, 130.0, 131.3, 132.4, 132.8, 132.9, 137.0, 137.1, 137.2, 139.1, 140.2, 141.8; FAB-MS  $m/z$  1550 ( $\text{M}^+$ ). Anal. Calcd for  $\text{C}_{122}\text{H}_{86}$ : C, 94.41; H, 5.59. Found: C, 94.18; H, 5.75.

**General Procedure for the 2-Fold Coupling of 3,3'-Diethynylbimesityl with Aryl Bromide via Sonogashira Coupling.** A typical procedure for the synthesis of **2** is as follows. Sonogashira coupling is described below for the synthesis of **2** as a representative case.

An oven-dried pressure tube was charged with 3,3'-diethynylbimesityl (0.45 g, 1.57 mmol), **15** (1.88 g, 5.66 mmol),  $\text{Pd}(\text{PPh}_3)_4$  (0.145 g, 8 mol%),  $\text{CuI}$  (0.006 g, 4 mol%), and  $\text{Et}_3\text{N}:\text{THF}$  (20:10 mL) under a  $\text{N}_2$  atmosphere and sealed. The contents were heated in an oil bath at 90 °C for 48 h. The reaction mixture turned yellow in color within 10 min and then to yellow-brown with time. After the usual workup, a short pad filtration over silica gel was performed with petroleum ether to isolate the unreacted 9-bromo-10-phenylanthracene and 9-phenylanthracene. Further elution with chloroform yielded a mixture of mono- and dicoupled products. Careful silica gel column chromatography of the mixture with 10% dichloromethane in petroleum ether led to a small amount of the monocoupled product first (10–15%) followed by the required difunctionalized bimesitylene **2** as a bright yellow solid. It was further purified by precipitation of its solution in dichloromethane/chloroform using ethanol, yield 0.63 g (51%):  $^1\text{H}$  NMR (500 MHz,  $\text{CDCl}_3$ )  $\delta$  2.04 (s, 6H), 2.47 (s, 6H), 2.83 (s, 6H), 7.20 (s, 2H), 7.37–7.45 (m, 10H), 7.54–7.61 (m, 8H), 7.68 (d,  $J = 8.5$  Hz, 4H), 8.86 (d,  $J = 9.0$  Hz, 4H);  $^{13}\text{C}$  NMR (125 MHz,  $\text{CDCl}_3$ )  $\delta$  19.1, 20.4, 21.9, 94.4, 99.5, 118.4, 121.6, 125.5, 126.2, 127.0, 127.4, 127.6, 128.4, 129.0, 130.0, 131.2, 132.1, 136.4, 137.4, 138.0, 138.1, 138.6, 139.1; FAB-MS  $m/z$  790 ( $\text{M}^+$ ); HRMS  $m/z$  calcd for  $\text{C}_{62}\text{H}_{46}$  790.3600, found 790.3616 ( $\text{M}^+$ ). Anal. Calcd for  $\text{C}_{62}\text{H}_{46}$ : C, 94.14; H, 5.86. Found: C, 94.19; H, 5.67.

**Synthesis of 3.** This compound was prepared by following the general procedure described above. **17** was used as the coupling partner with  $\text{Pd}(\text{PPh}_3)_4$  (8 mol%) as the catalyst. Isolation via silica gel column chromatography and purification as described above for **2** yielded **3** in 62% yield, bright orange fluorescent solid:  $^1\text{H}$  NMR (500 MHz,  $\text{CDCl}_3$ )  $\delta$  2.03 (s, 6H), 2.45 (s, 6H), 2.82 (s, 6H), 7.20 (s, 2H), 7.42–7.48 (m, 6H), 7.60–7.66 (m, 8H), 7.77–7.79 (m, 4H), 8.69–8.71 (m, 4H), 8.79–8.81 (m, 4H);  $^{13}\text{C}$  NMR (125 MHz,  $\text{CDCl}_3$ )  $\delta$  19.1, 20.4, 21.9, 86.6, 94.4, 101.1, 102.2, 118.0, 119.4, 121.5, 123.5, 126.7, 126.8, 127.3, 127.4, 128.6, 128.7, 129.2, 131.7, 132.0, 132.1, 136.7, 137.4, 138.2, 139.2; FAB-MS  $m/z$  838 ( $\text{M}^+$ ); HRMS  $m/z$  calcd for  $\text{C}_{66}\text{H}_{46}$  838.3600, found 836.3610 ( $\text{M}^+$ ). Anal. Calcd for  $\text{C}_{66}\text{H}_{46}$ : C, 94.47; H, 5.53. Found: C, 94.26; H, 5.70.

**Synthesis of 5.** This compound was prepared starting from 3,3',5',5'-tetraethynylbimesityl by following the general procedure described above. **15** was used as the coupling partner with  $\text{Pd}(\text{PPh}_3)_4$  (10 mol%) as the catalyst. With a short pad filtration of the reaction mixture over silica gel using petroleum ether, the unreacted 9-bromo-10-phenylanthracene and dehalogenated 9-phenylanthracene were isolated. Further filtration with  $\text{CHCl}_3$  yielded a mixture of products, which was subjected to  $\text{SiO}_2$  column chromatography. Gradual elution with 2–10% chloroform/petroleum ether led to a more polar component, which was identified as the required bimesitylene **5**. Further purification was accomplished via precipitation of its solution in dichloromethane/chloroform, yield 59%, bright yellow fluorescent solid: IR (KBr,  $\text{cm}^{-1}$ ) 2921, 2362, 2183, 1435, 1024;  $^1\text{H}$  NMR (400 MHz,  $\text{CDCl}_3$ )  $\delta$  2.68 (s, 12H), 3.39 (s, 6H), 7.44 (m, 16H), 7.61 (m, 20H), 7.72 (d,  $J = 8.8$  Hz, 8H), 8.93 (d,  $J = 8.8$  Hz, 8H);  $^{13}\text{C}$  NMR (100 MHz,  $\text{CDCl}_3$ )  $\delta$  19.9, 21.5, 94.9, 99.0, 117.0, 118.0, 122.7, 125.6, 126.4, 126.9, 127.5, 127.6, 128.4, 130.0, 131.1, 132.3, 138.4, 138.5, 138.6, 141.5;

FAB-MS  $m/z$  1344 ( $\text{M} + 1$ ). Anal. Calcd for  $\text{C}_{106}\text{H}_{70}$ : C, 94.75; H, 5.25. Found: C, 94.32; H, 5.53.

**Synthesis of 6.** This compound was prepared starting from 3,3',5',5'-tetraethynylbimesityl by following the general procedure described above. **16** was used as the coupling partner with  $\text{Pd}(\text{PPh}_3)_4$  (10 mol%) as the catalyst. Isolation and purification were carried out as described for **5** above, yield 52%, deep yellow fluorescent solid: IR (KBr,  $\text{cm}^{-1}$ ) 2920, 2179, 2050, 1607, 1511, 1435, 1245, 1032, 765;  $^1\text{H}$  NMR (500 MHz,  $\text{CDCl}_3$ )  $\delta$  2.66 (s, 12H), 3.38 (s, 6H), 3.96 (s, 12H), 7.14 (d,  $J = 8.5$  Hz, 8H), 7.37 (d,  $J = 8.5$  Hz, 8H), 7.43 (t,  $J = 8.0$  Hz, 8H), 7.66 (t,  $J = 8.0$  Hz, 8H), 7.77 (d,  $J = 9.0$  Hz, 8H), 8.90 (d,  $J = 9.0$  Hz, 8H);  $^{13}\text{C}$  NMR (125 MHz,  $\text{CDCl}_3$ )  $\delta$  19.9, 21.5, 55.4, 95.0, 99.0, 113.9, 117.8, 122.7, 125.5, 126.4, 126.9, 127.6, 130.3, 130.5, 132.3, 132.4, 137.9, 138.3, 138.6, 141.5, 159.2; FAB-MS  $m/z$  1463 ( $\text{M}^+$ ). Anal. Calcd for  $\text{C}_{110}\text{H}_{78}\text{O}_4$ : C, 90.26; H, 5.37; O, 4.37. Found: C, 89.48; H, 5.60.

**Synthesis of 7.** This compound was prepared starting from 3,3',5',5'-tetraethynylbimesityl by following the general procedure described above. **17** was used as the coupling partner with  $\text{Pd}(\text{PPh}_3)_4$  (10 mol%) as the catalyst. Isolation and purification were carried out as described for **5** above, yield 54%, bright orange red powder: IR (KBr,  $\text{cm}^{-1}$ ) 2922, 2367, 2182, 1597, 1435, 1023, 758;  $^1\text{H}$  NMR (500 MHz,  $\text{CDCl}_3$ )  $\delta$  2.64 (s, 12H), 3.36 (s, 6H), 7.43–7.48 (m, 12H), 7.67–7.70 (m, 16H), 7.80–7.81 (m, 8H), 8.73–8.75 (m, 8H), 8.85–8.87 (m, 8H);  $^{13}\text{C}$  NMR (125 MHz,  $\text{CDCl}_3$ )  $\delta$  19.9, 21.6, 86.5, 95.1, 100.4, 102.5, 118.5, 118.9, 122.6, 123.4, 126.8, 127.0, 127.3, 127.4, 128.6, 128.7, 131.7, 132.2, 138.9, 141.8; FAB-MS  $m/z$  1439 ( $\text{M}^+$ ). Anal. Calcd for  $\text{C}_{114}\text{H}_{70}$ : C, 95.10; H, 4.90. Found: C, 95.72; H, 4.83.

**PL Quantum Yield Measurements in Solutions.** For determination of fluorescence quantum yields, the solutions of bimesitylene-based EMs **1–7** were prepared in cyclohexane (spectral grade) such that their absorbance at  $\lambda = 367$  nm was ca. 0.025. These solutions were deaerated using nitrogen gas before their fluorescence was recorded at 298 K. The excitation wavelength was chosen as 367 nm for all the samples, and the emission in each case was recorded in the right angle mode (375–650 nm). The quantum yield was calculated from the following relation:

$$\phi_u = \phi_s(A_s/A_u)(I_u/I_s)(\eta_u/\eta_s)^2 \quad (1)$$

where the subscripts “s” and “u” refer to standard and unknown samples,  $A_u$  and  $A_s$  to absorbances of the sample and the standard at the excitation wavelength,  $I_u$  and  $I_s$  to the integrated emission intensities (i.e., areas under the emission curves) of the sample and the standard, and  $\eta_u$  and  $\eta_s$  to the refractive indexes of the corresponding solutions (pure solvents are assumed). Anthracene was chosen as a reference for quantum yield determination, for which the reported quantum yield in ethanol is 0.27.<sup>16</sup>

**Electrochemical Measurements.** The cyclic voltammetry experiments were performed on a BAS-100 B electrochemical analyzer. The data were collected and analyzed using electrochemical analysis software. All experiments were carried out in a three-electrode compartment cell with a Pt wire counter electrode, a glassy carbon working electrode, and a  $\text{Ag}/\text{AgNO}_3$  (0.1 M) reference electrode at varying scan rates. The supporting electrolyte used was 0.1 M tetrabutylammonium hexafluorophosphate solution in dry dichloromethane. The cell containing the solution of the sample (1 mM) and the supporting electrolyte was purged with a nitrogen gas thoroughly before scanning for its oxidation and reduction properties. For each determination, the CV was run independently for ferrocene as a reference. The oxidation potentials of **1–7** were subsequently determined from the average of the anodic and cathodic peak potentials and were corrected according to the values observed for ferrocene oxidation. The HOMO and LUMO values were thus calculated with reference to the ferrocene oxidation potential by using the following equations:  $E_{\text{HOMO}} = E_{\text{ox}} + 4.8$  eV;  $E_{\text{LUMO}} = E_{\text{HOMO}} - E_{\text{g}}^{\text{opt}}$ . The HOMO of ferrocene lies at 4.8 eV.

**Fabrication and Characterization of OLEDs.** The multilayer OLEDs were fabricated by employing the anthracene-anchored bimesitylenes as emitting materials. The ITO-coated glass substrates (Merck Display Technology, Taiwan) with a sheet resistance of  $<50 \Omega/\text{sq}$  were cleaned sequentially in an ultrasonicator using acetone, detergent solution, deionized water, ethanol, and 2-propanol and then subjected to oxygen plasma.

**Spin-Coating.** The commercially available solution of PEDOT (Bayer) was filtered using syringe filters of  $0.45 \mu\text{M}$ . A PEDOT layer of  $400 \text{ \AA}$  thickness was spin-coated onto the ITO glass substrate and dried at  $100 \text{ }^\circ\text{C}$  for 1 h under a vacuum. Further, a blend of PVK and anthracene-functionalized bimesitylenes (5–25 wt % **4** and **5**) in chlorobenzene (5 mL) was spin-coated above the PEDOT layer (2000 rpm for 30 s) and dried at  $50 \text{ }^\circ\text{C}$  overnight in vacuo. The ITO glass was transferred to the vacuum deposition chamber (ULVAC cryogenics) and sealed under a vacuum. Subsequently, the layers of TPBI or BCP/AIQ, LiF, and Al were deposited under a pressure of  $10^{-6}$  Torr at a rate of  $0.1\text{--}1.0 \text{ \AA}/\text{s}$ . The devices were sealed under an inert atmosphere in a glovebox, and the EL characteristics were measured.

**Vacuum Deposition.** Vacuum deposition of the organic materials such as NPB, 1% **1/2/8/9/10** with MADN, TPBI, LiF, and Al was carried out under a pressure of  $10^{-6}$  Torr on top of an etched ITO glass substrate sequentially. The rate of deposition of organic materials was maintained in a range of  $0.1\text{--}0.5 \text{ \AA}/\text{s}$ . The evaporation rate and thickness of the organic layers were monitored by a quartz oscillator. After the vacuum deposition, the devices were sealed, under an inert atmosphere, in a glovebox. EL spectra of the devices were obtained using a diode-array rapid analyzer system.

**Electroluminescence Measurements.** Current–voltage and light intensity measurements were performed on a Keithley 2400 source meter and a Newport 1835C optical meter equipped with a Newport 818-ST silicon photodiode, respectively. The device was placed close to the photodiode such that all the forward light entered the photodiode. The effective size of the emitting diode was  $4.0 \text{ mm}^2$ , which is significantly smaller than the active area of the photodiode detector, a condition known as “underfilling”, satisfying the measurement protocol.<sup>33</sup>

**Acknowledgment.** J.N.M. is thankful to the Department of Science and Technology (DST), India, for generous financial support. P.V.K. gratefully acknowledges the research fellowship from the CSIR, India. P.N. acknowledges the research fellowship from the UGC, India. We are thankful to the anonymous reviewers for their invaluable suggestions and criticism.

**Supporting Information Available:** Synthesis of starting materials and their spectral data,  $^1\text{H}$  and  $^{13}\text{C}$  NMR spectra of all the compounds, PL spectra (film), X-ray powder diffraction profiles, and EL data (EL spectrum of PVK-doped devices, luminescence, and external quantum efficiencies). This material is available free of charge via the Internet at <http://pubs.acs.org>.

JA8042905

(32) For example, see: Kido, J.; Hongawa, K.; Nagai, K. *Macromol. Symp.* **1994**, *84*, 81.

(33) Forrest, S. R.; Bradley, D. D. C.; Thompson, M. E. *Adv. Mater.* **2003**, *15*, 1043.